EFFECT OF SUPERCRITICAL WATER ON COKE FORMED DURING DODECANE CRACKING WITH ZSM-5

by

Patricia Guerra

A Thesis

Submitted to the Faculty

of the

WORCESTER POLYTECHNIC INSTITUTE

in partial fulfillment of the requirements for the

Degree of Master of Science

in

Chemical Engineering

September 2018

ABSTRACT

The objective of this work was to study the effect of supercritical water on coke formed on ZSM-5 during its use as a dodecane cracking catalyst. ZSM-5 coking was quantified at different reaction times, finding that the presence of supercritical water reduced coke formation by an order of magnitude or more. Coked samples were analyzed using several methods, including temperature programmed oxidation (TPO), attenuated total reflectance infrared (ATR-IR) spectroscopy, carbon-13 nuclear magnetic resonance (13C NMR), diffuse reflectance ultraviolet-visible spectroscopy (DR-UV-vis) and UV-Raman. Coked produced in the absence of SCW was formed by polycyclic aromatic hydrocarbons (PAHs) with more than 4 aromatic rings containing alkyl side chains. Coke produced in the presence of SCW was formed by aromatics with 1 to 3 aromatic rings. The characteristics of coke formed in the absence of water on ZSM-5 that had been pretreated in SCW were intermediate to those of coke formed on fresh ZSM-5 in the presence and absence of water, suggesting that the presence of water influences coke properties. It was also verified that SCW can decrease coke formation due to its effect on Bronsted acidity of the catalyst and ability to promote coke gasification. The effect of coke deposits produced in the presence and absence of SCW on the rate of ethanol dehydration, a model reaction studied under diffusion-controlled conditions, indicated that SCD/SWC coke deactivated less the catalyst than SCD coke.

Keywords: Coke, supercritical water, ZSM-5, zeolite, dodecane cracking

ACKNOWLEDGEMENTS

I would like to acknowledge Worcester Polytechnic Institute and the Chemical Engineering Department for the realization of this work.

I also thank National Council for Scientific and Technological Development (CNPq) from Brazil for the financial support.

I am very grateful to the professors of Worcester Polytechnic Institute and in special professor Michael Timko and the members of my committee.

I would like also to mention the cooperation of professor Geoff Tompsett and all the members of Timko Group.

Finally, I would like to thank my family for the assistance and encouragement during the execution of my Master`s program.

TABLE OF CONTENTS

LIST OF TABLES

LIST OF FIGURES

NOMENCLATURE

SBU	Secondary building units
SCW	Supercritical water
ATR	Attenuated total reflectance
TPO	Temperature programmed oxidation
DR-UV-vis	Diffuse reflectance ultraviolet-visible spectroscopy
NMR	Nuclear magnetic resonance
WHSV	Weight hourly space velocity
MTG	Methanol-to-Gasoline
TOS	Time on stream
GC	Gas chromatograph
FID	Flame ionization detector
TCD	Thermal conductivity detector
IR	Infrared spectroscopy
TGA	Thermogravimetric analysis
BAS	Bronsted acid site
SCD	Supercritical n-dodecane
PHAs	Polycyclic aromatic hydrocarbons
TOF	Turnover frequency

CHAPTER 1

INTRODUCTION

1.1 Introduction

Zeolites are crystalline materials composed of SiO_4 and $[AlO_4]^-$ tetrahedra. The negative charge of $[AlO_4]^-$ tetrahedra needs to be compensated by a cation to ensure electroneutrality. When this cation is H^+, the Bronsted acid sites are formed and render the zeolite high acidity. These materials also have high surface area and multidimensional microporous with molecular dimensions that can create shape-selectivity.

Zeolites have been used often in the petrochemical industry, where crude oil is converted into valuable fuels. In cracking, zeolites are used to break large molecules into smaller, which enhances the yield and quality of fuel. Liu et al. [1] prepared hierarchical HZSM-5 zeolites for cracking of n-dodecane carried out at 500 °C and 4 MPa in a tubular reactor. They observed an increase higher than 20% in the conversion of n-dodecane with the hierarchical catalyst and concluded that this was due to a better diffusion and acid site accessibility in the prepared HZSM-5. Lv et al. [2] synthesized hierarchically structured ZSM-5 zeolites with phosphorus incorporated by impregnation for testing on the cracking of 1-butene using a continuous flow microreactor operated at temperature of 550 °C and weight hourly space velocity (WHSV) of 10 h^{-1}. The authors found that the auxiliary mesopores and phosphorus modification improved selectivity (~52%) and yield (~43%) of propylene. In hydrocracking, a bifunctional catalyst, formed by a metal supported on a zeolite, is used in the presence of hydrogen and heat to process heavy feedstock. The metal site is used

for hydrogenation and dehydrogenation and the acidic support is important for skeletal isomerization generating carbenium ions. However, this process is considered expensive due to the amount of hydrogen required. Alsobaai et al. [3] studied the hydrocracking of petroleum gas oil using NiW/USY catalysts with different nickel (0–10.4 wt.%) and tungsten (0–30 wt.%) loadings prepared by impregnation in a high-pressure shaking reactor. The reactions were performed at 450 ◦C, contact time of 90 min and catalyst to gas oil ratio of 0.04. The authors found that the optimum content of nickel was 5 wt.%, which provided a conversion of 63.3 wt.% and yield of total distillate fuels (gasoline, kerosene, diesel) of 52.3 wt.%. They also observed that when the amount of tungsten increased the values of conversion and yield of total distillate fuels passed to 68.7 and 51.4 wt.%, respectively. Meng et al. [4] performed the hydrocracking of low-temperature coal tar over NiMo/Beta-KIT-6 catalyst on a fixed-bed reactor to produce gasoline. At the optimum condition, which was temperature of 385 °C, pressure of 80 bar, WHSV of 0.5 h^{-1} and H_2/oil of 800, the yield of gasoline fraction (≤180 °C) was 88 wt.%. The sulfur and nitrogen contents found in the gasoline were 50 and 20 mg kg^{-1}, respectively. The octane value of the gasoline was 79. In reforming, a bifunctional catalyst is used to increase the octane number of the gasoline. Zheng et al. [5] performed the aromatization of n-hexane using Pt/KL and Pt/Kβ catalysts in a flow microreactor. At the reaction conditions, which was temperature of 500 °C, pressure of 1 bar, WHSV of 2.2 h^{-1}, the authors found that Pt/Kβ showed more activity for skeletal isomerization and cracking, while Pt/KL showed superior aromatization activity. In terms of sulphur poising sensitivity, Pt/Kβ was stable to it. Chen et al. [6] prepared Zn-containing HZSM-5 by ion exchange and physically mixing methods for testing on ethylene aromatization using a flow fixed-bed reactor. They found Zn(OH)+ and ZnO species introduced on HZSM-5. At the reaction conditions,

which was temperature of 480 °C, pressure of 1 bar, WHSV of 0.9 h^{-1}, the authors identified that aromatics selectivity was improved with the introduction of Zn. $Zn(OH)^+$ acted as active sites for the dehydrogenation reaction, while ZnO was active for both dehydrogenation and hydrogenation reactions, allowing it to influence the amount of Bronsted acid sites required. In isomerization, a bifunctional catalyst is also used to improve gasoline efficiency. Bauer et al. [7] modified nano-crystalline Pt/HZSM-5 with pre-coking and liquid phase deposition of organosilane for xylene isomerization using a fixed-bed microreactor at 400 °C. The authors found higher product selectivity for the pre-coked catalyst and they considered that this treatment promoted selective passivation of external acid sites, which were mainly responsible for undesired disproportionation products (toluene and trimethylbenzenes). Barsi et al. [8] prepared bifunctional monometallic (Ni or Pt) and bimetallic catalysts (Pt-Ni) supported on HUSY zeolite by ion exchange method for n-hexane isomerization using a fixed-bed microreactor at 250 °C and 1 bar. The authors found that the bimetallic catalysts presented a higher activity than the monometallic and that the activity achieved a maximum when Pt content was equal to or higher than 50%. Alkylation is another process where zeolites are used to produce high octane gasoline. Yoo et al. [9] studied the alkylation of isobutane with 2-butene using different large-pore zeolites (USY, mordenite, beta, LTL, and ZSM-12). The reaction conditions were temperature of 80 °C, pressure of 20 bar and WHSV of 0.1 h^{-1}. They observed better coke tolerance over ZSM-12 (one dimensional) than USY (three dimensional) and higher activity and selectivity to the desired products for samples synthesized with low Si/Al ratios due to the high hydrogen transfer capability of these samples. Nivarthy et al. [10] investigated the alkylation of isobutane with ethene and propene over an H-BEA catalyst in a well-stirred reactor. The reaction conditions were temperature of 75 °C, pressure of 30 bar

and WHSV of 0.2 h^{-1}. The authors found that only with propene single alkylation occurred and iso-heptanes were the dominant products. Zeolite-based ZSM-5 catalysts are either crucial to Mobil's Methanol-to-Gasoline (MTG) process. Shao et al. [11] hydrothermally synthesized ZSM-5 with different crystal size (70, 200, 400 and 650 nm) and tested it for conversion of methanol to gasoline using a fixed-bed reactor at temperature of 400 °C, pressure of 10 bar and WHSV of 4.74 h^{-1}. The authors concluded that the catalytic lifetime and the liquid hydrocarbon yield decreased with increasing ZSM-5 crystal size. They showed that ZY5-70 sample had the longest catalytic lifetime of 96 h with the highest liquid hydrocarbon yield of 30.8 %. Soltanali et al. [12] investigated the effect of pressure (1-11 bar), temperature (350-400 °C), weight hourly space velocity (1-5 h^{-1}) and catalyst particle size (90, 2000 and 4000 nm) on gasoline selectivity in methanol to gasoline conversion process using a fixed-bed reactor and applying experimental design. The optimal conditions to achieve maximum gasoline selectivity were pressure of 9.40 bar, temperature of 392 °C, WHSV of 1 h^{-1} and particle size of 994 nm. Zeolites have also application in bioenergy, where biomass is transformed in renewable fuels through catalytic fast pyrolysis and upgrading processes, which can contribute to solve the fossil fuels shortage and environmental issues. Li et al. [13] studied the catalytic fast pyrolysis of Kraft lignins for producing aromatics in the absence and presence of HZSM-5 in a Curie-point pyrolyzer. Without the catalyst, fast pyrolysis of lignin predominantly produced phenols and guaiacols. However, in the presence of HZSM-5 the lignin-derived oxygenates progressively decreased to trace and the aromatics increased considerably. Under optimal reaction conditions, the aromatic yield was 2.0 wt.% for one lignin and 5.2 wt.% for the other. Zhang et al. [14] investigated the catalytic pyrolysis of willow wood in a fluidized bed reactor using metal-loaded (Mg, K, Fe, Ga, and Ni) ZSM-5. The results showed that

bio-oil yields with metal-loaded catalysts (40 to 43.4 wt.%) were a little lower than that of pure ZSM-5 (46.4 wt.%). The synthesized catalysts loaded with Ga, Fe, or Ni improved the percentages of benzene, toluene, and xylenes in bio-oils. Ga/ZSM-5 showed the highest relative content of toluene (37.4%), while Ni/ZSM-5 showed the highest relative content of xylenes (27.3%). Fe/ZSM-5 produced the highest relative content of benzene (17.9%). Metal-loaded catalysts produced more CO2 and CO than pure ZSM-5. Fe/ZSM-5 produced the highest yield of olefins (2.7 wt.%). Anand et al. [15] studied the catalytic fast pyrolysis of Spirulina platensis, a species of microalgae, using different zeolites (ZSM-5, Beta and Y) in a micropyrolyzer. They observed that increasing catalyst loading (2:1 to 50:1 wt./wt.) and temperature (350 to 600 °C) elevated the formation of monoaromatics, polyaromatics and cycloalkanes. They also noticed the generation of nitriles from dehydration of amides originally present in algae. The nitriles production increased with catalyst loading and decreased with temperature. Bambang et al. performed integrated pyrolysis and upgrading processes of bio-oil using Cu-modified Beta zeolite in a fixed-bed reactor at 600 °C. The results showed that when 0.50 wt.% of Cu is loaded on the catalyst by impregnation almost only hydrocarbons could be detected in the light oil of upgraded bio-oil and it also contributed to decrease coke deposition on the catalyst. This increase in activity was due to a synergetic effect between the doped metal sites and the proton sites on the zeolite structure. The authors also verified that this loading of Cu increased surface area and promoted formation of more micropores on the catalyst. Kim et al. [16] investigated the catalytic pyrolysis of Citrus unshiu peel and the posterior catalytic upgrading of the pyrolyzates, which were mainly alcohols, ketones and furans. The authors verified high aromatic yield for HZSM-5 and HBETA, however the last generated large amounts of undesirable polyaromatics.

The main problem associated with the use of zeolites is its deactivation by coke formation, which can cause pore blockage of the catalyst and acid sites poising. Coke deposits on the catalyst can also require the construction of expensive regeneration units to restore the catalyst performance. Wang et al. [17] studied the deactivation of HUSY zeolite during the cracking of 1-pentene at 250-350 °C, 1 bar and WHSV of 86.211 h^{-1}. They observed that cracking and hydride transfer were the predominant reactions in the first minute of TOS (time on stream). After that, isomerization became the main reaction. During the deactivation of the catalyst, the amount of soft coke decreased with increasing reaction temperature due to it high volatility, while the amount of hard coke increased. Paweewan et al. [18] investigated the deactivation of HUSY zeolite during the cracking of n-hexane at 250-350 °C, 1 bar and WHSV of 86.211 h^{-1}. The authors found as main products propane and propene. It was also observed that only took a small amount of coke to have a large effect on catalytic activity. They noticed either that the coke produced presented high aromaticity. Lee et al. [19] studied the deactivation by coke deposition on the HZSM-5 (SiO_2/Al_2O_3 ratios of 40 and 280) in the methanol-to-hydrocarbon conversion. The tests were performed in a fixed-bed reactor at 500 °C, 1 bar and WHSV of 4.25 h^{-1}. They observed that at low acidity the coke formed was mainly mono- or bi-aromatic, while at high acidity the carbonaceous deposits were composed by polycyclic aromatics with 3 or 4 fused rings. Quereni et al. [20] explored the deactivation of Y-zeolite, mordenite and L-zeolite in the protonic form and after ion exchange with lanthanum nitrate during the isobutane alkylation with C4 olefins. The alkylation was performed in a fixed-bed reactor at 25-80 °C and using WHSV of 1 h^{-1}. The authors found that lanthanum-exchanged Y-zeolite showed the better activity and stability, however a high amount of coke was deposited on this catalyst (13-14%).

One alternative to minimize the catalyst deactivation by coke deposition is the operation in the presence of water. Supercritical water (SCW), for example, has been widely studied in the upgrading of hydrocarbons because above its critical point water become non-polar and can dissolve organic compounds. Han et al. [21] performed the upgrading of coal-tar pitch in SCW using a batch reactor at temperature (400-480 °C), pressure (250-400 bar) and residence time (1-80 min). The authors found a higher conversion of asphaltene to maltene compared with pyrolysis in nitrogen. They also emphasized that gas and char formation were restricted in SCW. Morimoto et al. [22] used SCW in the upgrading of oil sand bitumen in an autoclave at 420-450 °C and 200-300 bar for up to 120 min. The authors observed that SCW provided high conversion and low coke yield.

For thermal coke formation, where coke is formed in the absence of a catalyst and by radical reactions, the low coke yield was attributed to the fact that SCW could donate hydrogen and terminate free radicals known as coke precursors. Hydrogen-deuterium exchange data provided evidence for hydrogen supplied by water. Deuterium was incorporated into the products of hydrocarbon pyrolysis in supercritical D_2O. However, there is still some authors that did not support the hydrogen donor ability of SCW. They attributed the low coke formation due to the fact that asphaltenes, which are the main coke precursors in heavy oil, would be partially dissolved and dispersed in SCW as an emulsion; this would not only reduce the asphaltene concentration for coking, but also the coking reaction would be slowed down because of the mass-transfer resistance between different emulsion droplets [23,24].

In catalytic coke formation, where coke is formed in the presence of a catalyst and by an ionic mechanism, it was described that the presence of water in the form of steam also suppressed the production of coke and minor aromatic products. It was

suggested that steam dilution enhanced the desorption of coke precursors, diolefinic ions and cyclic ions, avoiding the further pathological reactions to produce aromatics and polyaromatics [25].

However, there is no study reporting the effects of SCW on catalytic coke formation and the impact of SCW-formed coke on ZSM-5 activity.

1.2 Research Objectives

The overall objective of this thesis was to investigate the effects of SCW on catalytic coke formation and the impact of SCW-formed coke on ZSM-5 activity. The specific aims were the following:

- ***Specific Aim 1:*** **SCW can affect coke quantity and chemical nature.** This hypothesis will be verified by analyzing the coke produced during the cracking of dodecane in the presence and absence of SCW over ZSM-5 for different times with several techniques. TPO will be used to measure coke amount, ATR-IR will be used to identify functional groups, solid-state ^{13}C NMR will use to examine carbon framework, DR-UV-vis will be used to understand the aromatic content of the coke and UV Raman will be used to evaluate clustering.

- ***Specific Aim 2:*** **SCW can decrease Bronsted acidity of ZSM-5, which will decrease coke formation.** This hypothesis will be verified by degrading the catalyst in SCW for different times and then using it in the cracking of only dodecane. The coked produced with the pretreated zeolites will be analyzed with TPO, ATR-IR and solid-state ^{13}C NMR.

- ***Specific Aim 3:*** **SCW can promote coke gasification in the presence of ZSM-5, which would decrease its quantity.** This hypothesis will be verified by gasifying coke in SCW at 400 °C and 24.8 MPa in the presence of ZSM-5 for 2 h. The gasified coke will be analyzed using TPO and the gases formed will be analyzed using GC-TCD.

- ***Specific Aim 4:*** **Coke deposits produced in the presence and absence of SCW can affect differently ZSM-5 activity.** This hypothesis will be tested by using the coked zeolite produced in the presence and absence of SCW in a model reaction such as ethanol dehydration chemistry and analyzing the activity of the catalyst in the presence of the coke deposits.

CHAPTER 2

LITERATURE REVIEW

2.1 Zeolites

Zeolites are crystalline aluminosilicates formed by a three-dimensional network of AlO_4 and SiO_4 tetrahedra linked together by oxygen atoms, as shown in Figure 1. The AlO_4 tetrahedra generates negative charges on the structure which are neutralized by compensation cations. When these cations are protons, the Bronsted acid of the zeolite is created, which is responsible for its high activity.

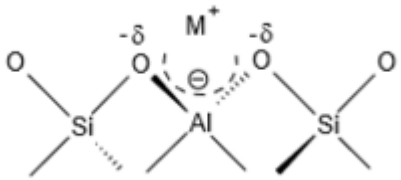

Figure 1 Structure of the tetrahedra [26]

The TO_4 tetrahedra can be organized in several ways, which will originate different zeolite frameworks and pore structures, as shown in Figure 2.

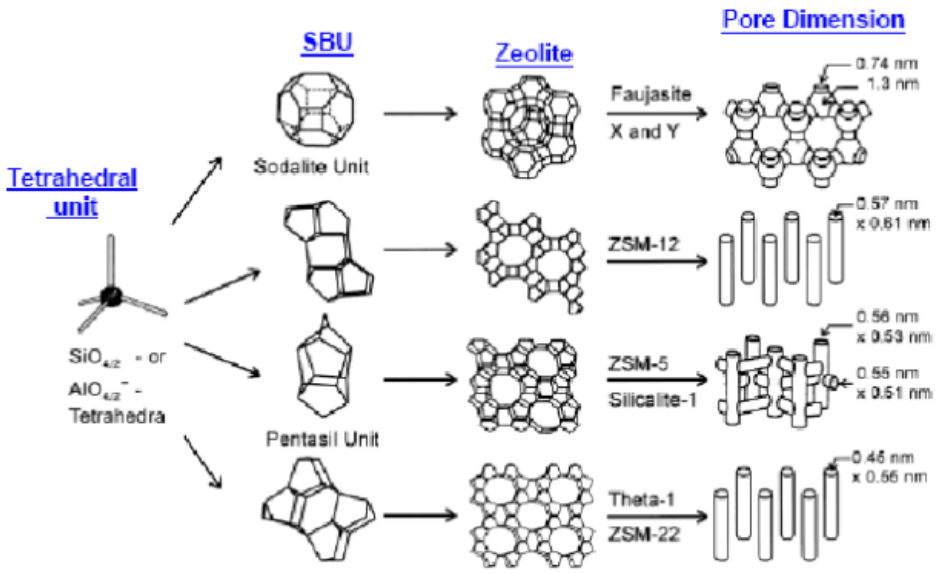

Figure 2 Framework and pore structure of different zeolites [26]

The crystalline structure of the zeolites creates a pore system that is responsible for high surface area and can limit the size and shape of the molecules that can enter or be formed inside of the pores, conferring high selectivity for reactions performed with zeolites.

Zeolites can be classified according to the pore diameter as shown in Table 1.

Table 1 Zeolite classification according to pore diameter [26]

Pore Size	Number of Tetrahedra (MR [1])	Pore Diameter (Å)	Example
Small	8	4	PST-1 (NAT)
Medium	10	5.5	ZSM-5 (MFI)
Large	12	7.5	ZSM-12 (MTW)
Extra-large	>12	>7.5	CIT-5 (CFI)

[1] MR: Members of the ring.

2.2 Coke Formation Mechanism

At low reaction temperatures, (< 200 ˚C), coke formation involves mainly condensation and rearrangement steps and the deposits are not polyaromatic.

At high temperatures (> 350 ˚C), the coke components are polyaromatic. In this case, olefins are converted into aromatics, which polymerize to polyaromatics, the coke constituents, as shown in Figure 3.

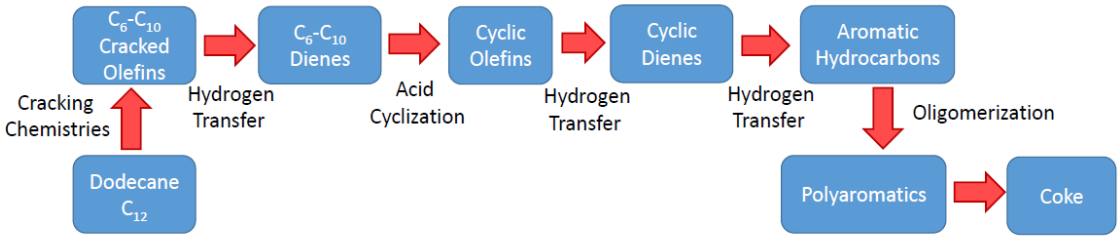

Figure 3 Mechanism of coke formation [27]

2.3 Coke Characterization Techniques

Infrared spectroscopy (IR) is frequently used to investigate the nature of the coke formed but other techniques such as ultraviolet-visible (UV-Vis) and nuclear magnetic resonance (NMR) can be chosen.

Thermogravimetric analysis (TGA) can be used to measure weight loss with increasing temperatures and it is an important technique to quantify coke and discriminate between different types of carbonaceous deposits.

Adsorption measurements can be used to characterize the coke deposition in the void volume of the zeolite and clarify if the coke is predominantly deposited inside the pores or on the external surface.

The chemical composition of the coke can be determined performing the extraction of the soluble coke components with dichloromethane and analyzing the extract with gas chromatograph (GC).

2.4 Coke Composition

Li et al. [28] studied coke formation on ZSM-5, USY and SAPO-34 zeolites during methanol conversion to olefins at temperatures from 25 to 500 °C using ultraviolet Raman spectroscopy and observed that the coke species formed on SAPO-34 were mainly polyolefin species and in ZSM-5 were aromatic species but polyaromatic or substituted aromatic species were predominant in USY at high temperatures. The main reason for the different behavior of coke formation in the three zeolites was attributed to the different pore structures of the zeolites. Du et al. [29] studied coke formation during pyrolysis of model compounds of bio-oil (toluene, toluene with propylene, tolualdehyde and furan) over ZSM-5 at 600 °C using a fixed bed reactor. They observed coke formation via oligomerization and polymerization of aromatic hydrocarbons and olefins. Catalytic pyrolysis of toluene and tolualdehyde produced coke with higher crystallinity, with a less condensed structure and containing significant amounts of aliphatic carbons. Among the model compounds studied, furan produced the most condensed form of coke with no aliphatic carbons. Cerqueira et al. [30] investigated coke formation during methylcyclohexane transformation over HFAU, HBEA and HMFI zeolites with Si/Al ratio of 15 using a fixed-bed reactor at

450 °C for several contact times. Coke formation was found to be much faster on HBEA than on HMFI due to the higher pore size of the HBEA. Coke was shown to be produced from the transformation of aromatic and olefinic products. At low contact times, coke was constituted by aromatic species soluble in CH_2Cl_2, while at higher contact times coke was formed by polyaromatic compounds insoluble in organic solvents.

CHAPTER 3

EXPERIMENTAL

3.1 Protocol for coke preparation

Coked ZSM-5 was prepared from the cracking of dodecane in the presence and absence of SCW. Reactions were performed in a 316-stainless steel Parr batch reactor with an internal volume of 100 mL. Reaction temperature and stirring rate were controlled by a Parr 4848 reactor controller. Reactions were performed by loading the reactor with pure dodecane or 50/50 wt% dodecane/water mixture. In all cases, ZSM-5 loading was 5% with respect to the initial dodecane mass and the Si/Al ratio of the ZSM-5 was 38. After reactor loading, the reactor was then purged 5 times with 3.5 MPa of He to remove residual air. For the reactions performed in the presence of water 1.7 MPa of He was then added to the reactor to ensure that the reaction mixture reached a pressure of 24.8 MPa after heating, while for the reactions in the absence of water 5.1 MPa of He was added. The reactor was then heated with mixing at 160 rpm to the desired temperature (400°C). After reaching the desired temperature, the reactor temperature was maintained for different reaction time (0 to 8 hours). Once the desired reaction time was reached, the reaction was quenched by submerging the reactor in cold water and depressurizing it. Reaction times of 0 hours indicated that the reactor was heated to the desired temperature and then immediately quenched. Heating the reactor to 400 °C required approximately 30 min. The reactor was opened and the coked catalyst was recovered by filtration, rinsed with dichloromethane and dried at 60 °C overnight. The reactor was weighted before the reaction, when it was loaded with the

reactants, catalyst and helium and after the reaction without the release of the gases formed to ensure that 100% of mass was conserved.

3.2 Protocol for coke analysis

Temperature-Programmed Oxidation (TPO) analysis was obtained in a TGA 209 F1 Libra from Netzsch. The samples were heated until 800 °C at 10 °C/min in an alumina crucible. The flow rate of oxygen was 4 mL/min and the flow rate of nitrogen was 8 mL/min. Analyses were performed in duplicate to confirm reproducibility (± 0.5%).

Attenuated Total Reflection Fourier Transform Infrared (ATR-IR) analysis was performed in a Vertex 70 Bruker spectrometer. The spectra were measured at a resolution of 4 cm^{-1} with 512 scans in a range between 4500 and 600 cm^{-1}. Analyses were performed in duplicate to confirm reproducibility and the final spectrum for each sample was the average of the two measurements.

Solid-state ^{13}C Nuclear Magnetic Resonance (NMR) with multiple cross-polarization (Multi CP) was performed according to the method introduced by Johnson and Schmidt-Rohr [31]. All the samples were packed into 4-mm zirconia rotors without further treatment. NMR spectra were measured using a Bruker Biospin DSX400 spectrometer at 100 MHz for 13C, using 14-kHz magic-angle spinning (MAS) of 4-mm rotors in double-resonance probe head.

Diffuse Reflectance UV-visible (DR-UV-vis) analysis was realized in a Thermo Scientific Evolution 300 spectrophotometer equipped with a Praying Mantis diffuse reflection cell. The white reflectance standard was $BaSO_4$. The spectra were plotted assuming the model of Kubelka and Munk for diffuse reflectance. Analyses were

performed in duplicate to confirm reproducibility and the final spectrum for each sample was the average of the two measurements.

Ultraviolet Raman spectroscopy was performed in a Renishaw confocal microscope using excitation beam of 244 nm. The samples were prepared for analysis by transferring a portion of each sample to stainless steel slide. The 244 nm UV laser operating on the Raman system had a maximum power of 5 mW at the sample. Analyses were performed in three sites of the sample and the final spectrum for each sample was the average of the three measurements.

3.3 Protocol for catalyst degradation in SCW

Degraded ZSM-5 was prepared by treating for either 0 and 2 h in SCW (without dodecane) at 400 °C and 24.8 MPa in a batch reactor.

3.4 Protocol for coke gasification in SCW

The gasification of the coked ZSM-5 was performed in a 316-stainless steel Parr batch reactor with an internal volume of 100 mL. Reaction temperature and stirring rate were controlled by a Parr 4848 reactor controller. In all experiments, the reaction temperature was 400 °C, the pressure approximately 24.8 MPa and the reaction time was 2 h. The reactor was pre-pressurized with He to ensure that the desired pressure was achieved when the reaction temperature was reached. Reactions were performed by loading the reactor with 2 g of coked zeolite (SDC coke produced in a 2 h reaction) and 40 mL of deionized water. Once the desired reaction time was reached, the reaction was quenched by submerging the reactor in cold water and the reactor was

depressurized. The reactor was then opened and the gasified coke was recovered by filtration, rinsed with dichloromethane and dried at 60 °C overnight for further analysis with TPO. Gas products released during depressurization were analyzed using a Shimadzu GC-2014 with a 1 µL sample-injection loop connected to a Hayesep Q column (length: 3m and inner diameter: 3.17 mm) and TCD detector operating at 150 ^{o}C and 120 mA. Helium was the carrier gas. The temperature program consisted of an initial temperature of 30 °C, followed by a 5 °C/min ramp to 90 °C with a 20 minutes hold, followed to a 10 °C/min ramp to 130 °C with a 40 minutes hold. The peaks in the chromatogram were identified by injecting standard mixtures of gases.

The reactor was weighted before the reaction, when it was loaded with coked zeolite, water and helium and after the reaction without the release of the gases formed to ensure that 100% of mass was conserved.

3.5 Protocol for evaluation of the coke deposits on ZSM-5 activity

The effect of coke deposits produced in the presence and absence of SCW on ZSM-5 activity was investigated by testing coked zeolites in ethanol dehydration reaction. The ethanol dehydration reaction in vapor phase was carried out in a flow reactor. The reaction conditions were: 100% of ethanol as feed, ethanol feed flow rate of 2 mL/min, temperature of 350 °C, atmospheric pressure and coked zeolite loading of 0.1 g. Reactant was stored within the reactor enclosure and pumped with a centrifugal pump. The reactant passed through a mixing block prior to entering the oven chamber. Upon entering the oven, reactant moved through a coil designed to allow it to reach full temperature before entering a packed bed reactor loaded with coked zeolite. The outlet

end of the reactor was blocked with a porous frit that allowed products to exit but retaining the coked zeolite packed bed.

Gas products were analyzed using a Shimadzu GC-2014 with a 1 µL sample-injection loop connected to a RT-Q-Bond (length: 30 m and inner diameter: 0.25 mm) and FID detector operating at 250 ^{o}C.

The temperature program consisted of an initial temperature of 150 °C with a 310 minutes hold. A calibration curve was built by analyzing mixtures with different volume percentages of ethylene in helium (the total flow rate used was 750 mL/min). The volume percentage of ethylene produced with the coked zeolites was converted in flow rate of ethylene, which was further converted in moles for the calculation of the yield. Yield was further used in the calculation of turnover frequency (TOF), which is a measure of catalyst activity. The equations used are shown below.

FR ethylene (mL/min) = 750 x V% ethylene

Moles ethylene = FR ethylene x density ethylene x 1/MW ethylene

Yield ethylene = Moles ethylene / Moles ethanol in the feed

TOF ethylene (g/min/site) = Reactant flow rate (g/min) x Yield /Quantity of sites (µmol/g) x Catalyst mass (g)

Coked zeolites were analyzed by TPO after being used in ethanol dehydration reaction to verify if the coke deposited on the catalysts remained stable during the process.

CHAPTER 4

RESULTS AND DISCUSSIONS

4.1. Specific Aim 1 - SCW can affect coke quantity and chemical nature

To investigate how SCW affects coke quantity and chemical nature, coke produced in the presence and absence of SCW was analyzed with different techniques.

The amount of coke for the reactions performed in the presence and absence of SCW was recorded using TPO analysis and is shown in Figure 4. It was observed that SCW reduced coke formation by an order of magnitude or more.

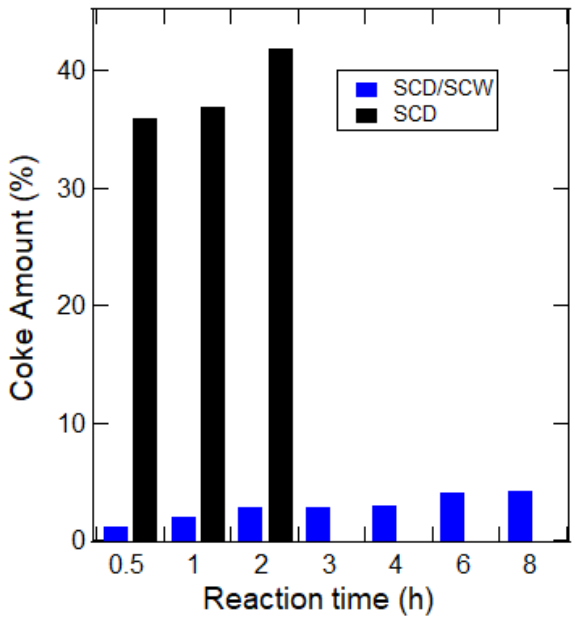

Figure 4 Coke quantification in the presence and absence of SCW

Figure 5 shows the coke amount for the reactions in the presence of SCW and in its absence plotted versus the normalized TPO temperature. It was observed higher

TPO temperatures for the coke produced in the absence of SCW, suggesting that this coke has a high polyaromatic character.

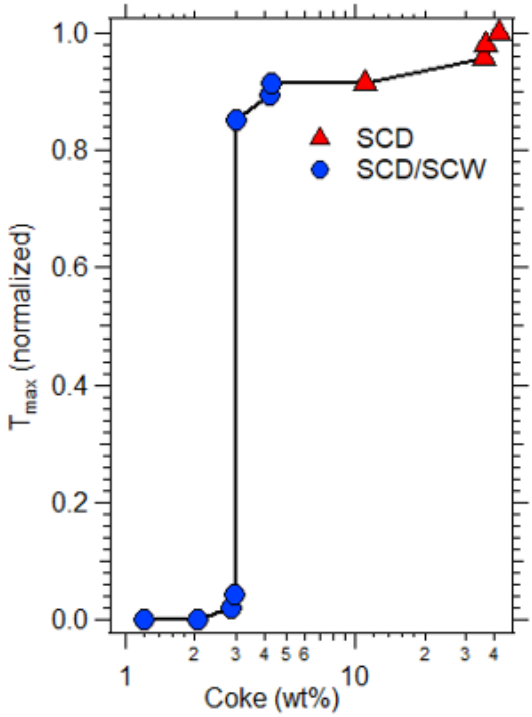

Figure 5 Coke quantification versus normalized TPO temperature

Solid-state ^{13}C NMR with multi cross-polarization (Multi CP) was used to examine the carbon framework. Figure 6a shows the Multi CP and Multi CP/Grade (non-protonated or mobile) ^{13}C NMR spectra for coke formed in the presence of SCW. Two major spectral regions could be identified: the peak at 130 ppm, which was associated with aromatic species and the peaks at 10–40 ppm, which were related with aliphatic carbon species from the reactant (dodecane) trapped inside the pores of the catalyst. Figure 6b shows the Multi CP and Multi CP/Grade (non-protonated or mobile) ^{13}C NMR spectra for the coke formed in the absence of SCW. It was verified that the

coke produced in the absence of SCW was highly aromatic with CH_3 bonded to aromatics. The olefin content detected was very low.

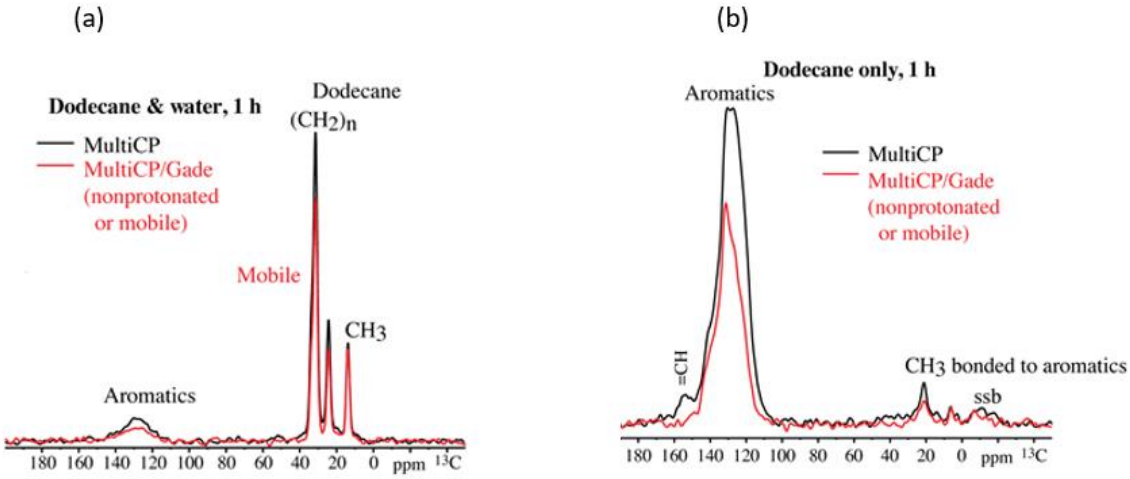

Figure 6 13C NMR spectra for (a) SCD/SCW coke and (b) SCD coke

ATR-IR was used to identify functional groups. Figure 7a shows the ATR-IR spectra obtained for the coke produced in the presence of SCW at different reaction times in C-C region. A prominent feature was observed at 1480 cm^{-1}, while a minor band was present at 1640 cm^{-1}. These bands were consistent with C-C aromatic stretches, however they are displaced from the usual locations observed for multi-ring PAHs and instead are consistent with single-ring aromatics. Another band was observed at 1720 cm^{-1} and was attributed to carbonyls. Because water was the only oxygen source in the reactor, it is possible to assume that water may play a chemical rule in coke formation. Figure 7b shows the ATR-IR spectra obtained for the coke produced in the absence of SCW in the C-C region. A prominent feature at 1610 cm^{-1} dominated the ATR-IR spectrum and was attributed to aromatic C-C stretches. A secondary feature at 1460 cm^{-1} was due to the Kekulé mode of aromatic molecules.

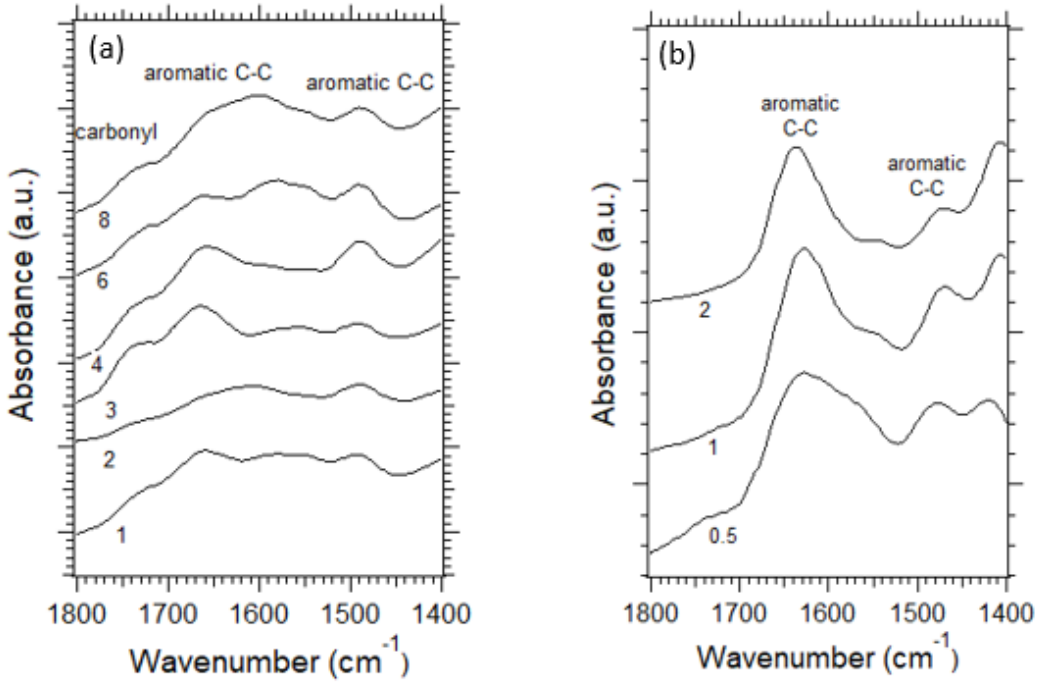

Figure 7 ATR-IR spectra for (a) SCD/SCW coke and (b) SCD coke in the C-C region

Figure 8a shows the ATR-IR spectra obtained for the coke produced in the presence of SCW in C-H region. It was observed that the spectrum is dominated by CH3 stretches and aromatic C-H stretches begin to become apparent at reaction times >6 hours. Figure 8b shows the ATR-IR spectra of the coke produced in the absence of SCW in the C-H region. In this case, it was verified that the C-H stretch region consisted primarily of a prominent band associated with aromatic C-H stretches; CH_3 stretches were also present.

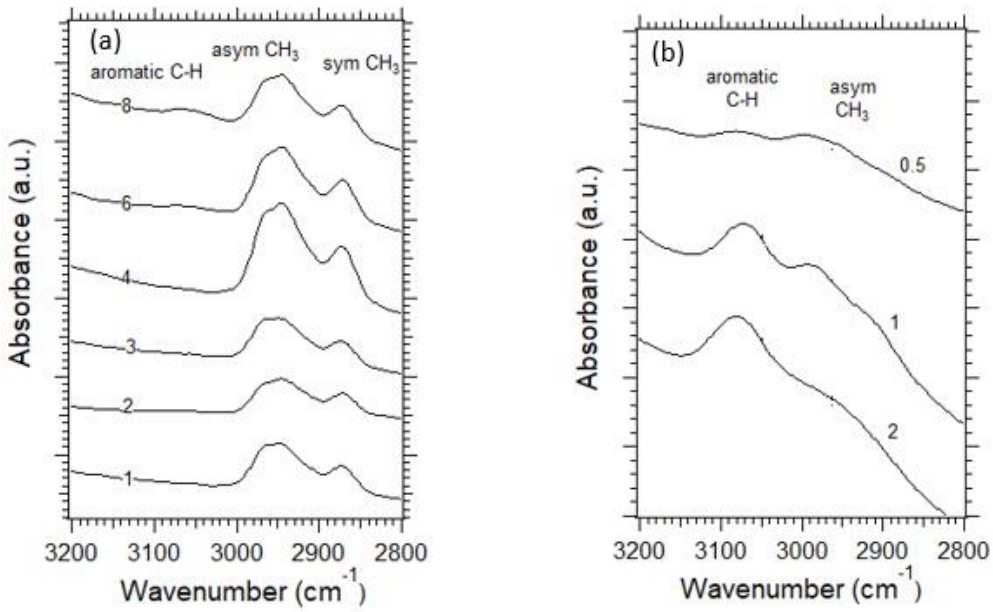

Figure 8 ATR-IR spectra for (a) SCD/SCW coke and (b) SCD coke in the C-H region

ATR-IR was also used for quantification of the vibrations observed. The spectra of the coke produced in the presence and absence of SCW in the C-H region were deconvoluted in several Lorentzian peaks with the following assignments: 2855 cm^{-1}, CH_2 (symmetric); 2900-2925 cm^{-1}, CH_2 (asymmetric); 2870 cm^{-1}, CH_3 (symmetric); 2955 cm^{-1}, CH_3 (asymmetric) and 3030 cm^{-1}, aromatic C-H [32]. The area of the peaks was used for quantification. One example of deconvolution is shown in Figure 9.

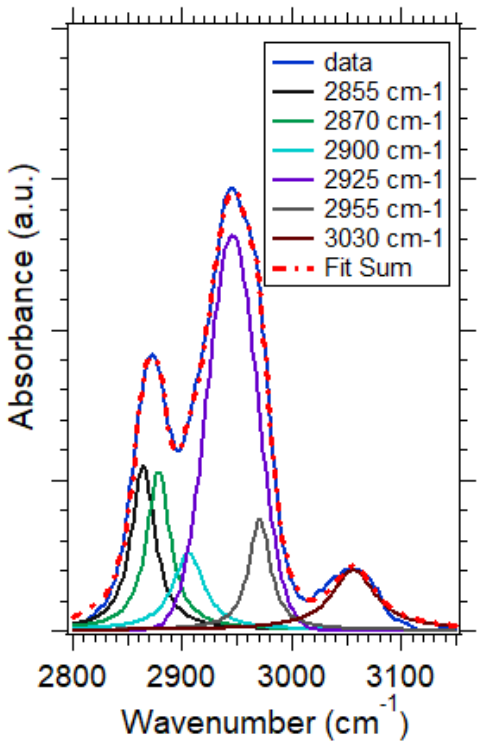

Figure 9 ATR-IR spectra for the SCD/SCW coke 8 h deconvoluted in Lorentzian peaks

Figure 10 shows a plot of aliphatic/aromatic versus coke amount. It was observed that the aliphatic content observed in the presence of SCW, which was due to dodecane trapped inside the pores of the catalyst, decreased when the coke amount increased. It was also clear that the coke produced in the absence of SCW was highly aromatic.

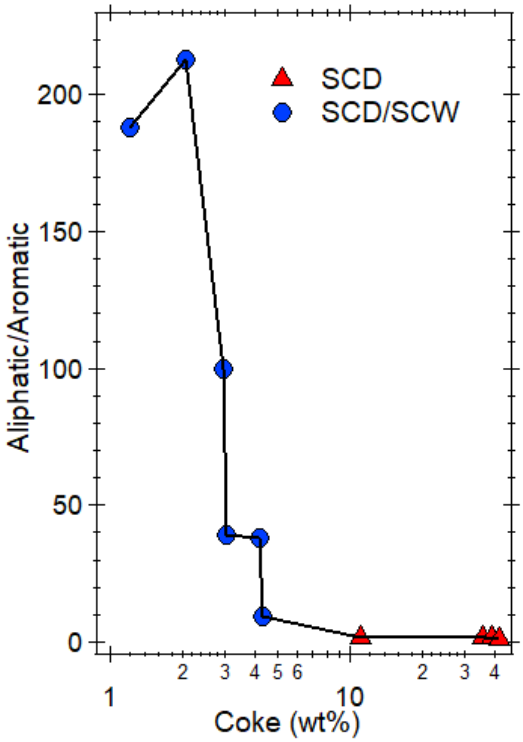

Figure 10 Aliphatic/Aromatic versus coke amount

Diffuse reflectance UV-vis spectroscopy (DR-UV-vis) was used to understand the aromatic content of coke formed in the presence and absence of SCW. In the literature for example, the UV-vis spectra in the 200-900 nm range of the coke deposited on HZSM-5, Hβ and HY zeolites during the cracking of polyethylene were deconvoluted in several vibrations. The authors found that a band at 375 nm increased in intensity with pore size (HY>Hβ>HZSM-5) and this band was attributed to conjugated double bonds and polycondensed aromatics with more than four aromatic rings. The authors also observed that as the micropore size of the zeolite increased, bands located at higher wavelength values (580–600, 780 and 820 nm) were also observed and were due to higher condensed polyaromatics [32].

Because it was not identified any band in the higher wavelength region for the analysis of the coke of this research, a simplified and more qualitative method for

deconvolution of the DR-UV-vis spectra was developed. The spectra of the coke produced in the presence and absence of SCW were deconvoluted in several Gaussian peaks with the following assignments: 255 nm (benzene), 286 nm (naphthalene), 375 nm (anthracene), 400-430 nm (PHAs with more than 4 aromatic rings). The area of the peaks was used for quantification. One example of deconvolution is shown in Figure 11.

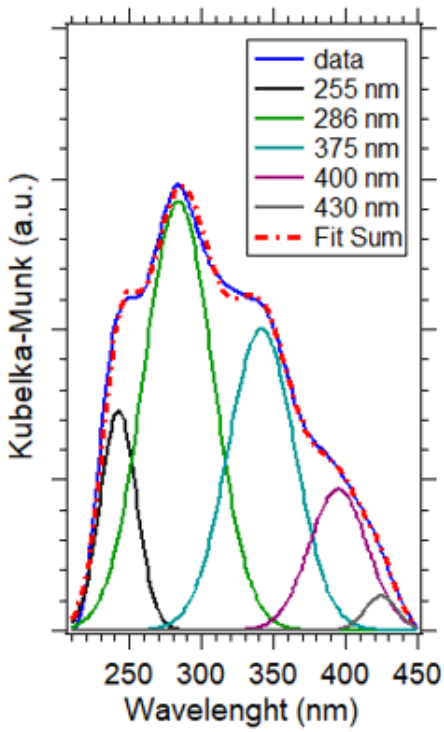

Figure 11 DR-UV-vis spectra for the SCD/SCW coke 8 h deconvoluted in Gaussian peaks

Figure 12 shows a plot of aromatic 1-3 rings/aromatic 4+ rings versus coke amount. It was noticed that the coke produced in the absence of SCW was formed by

PHAs with more than 4 aromatic rings, while the coke generated in the presence of SCW was constituted by aromatics with 1 to 3 rings.

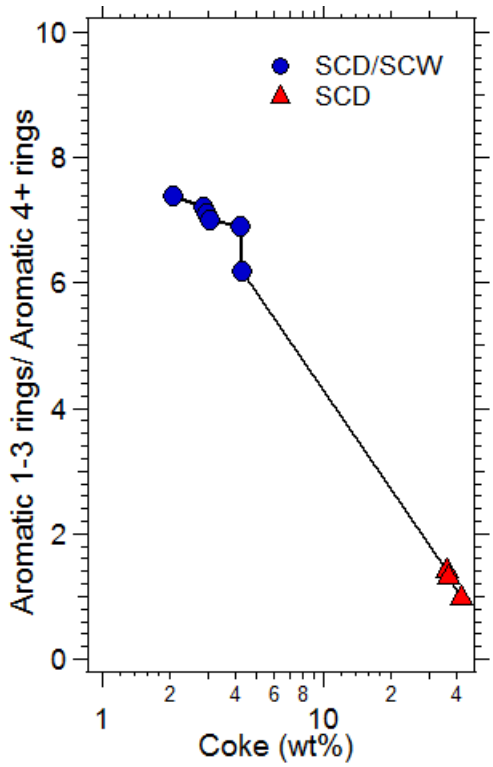

Figure 12 Aromatic 1-3 rings/Aromatic 4+ rings versus coke amount

Ultraviolet Raman was used to measure cluster size and to avoid the problem of fluorescence in the analysis of coked zeolites. In this case, ultraviolet light is used to excite the Raman scattering without generating the fluorescence. The UV-Raman spectra of the coke produced in the presence and absence of SCW have been deconvoluted in several Gaussian peaks with the following assignments: (i) the shoulder at 1250 cm^{-1} is identified as C–H vibrations; (ii) D1, caused by the "breathing" mode of poorly structured aromatic clusters, at 1380 cm^{-1}; (iii) D3, caused by the structural defects of these aromatic clusters, at 1450–1510 cm^{-1}; (iv) G, at 1575–1600 cm^{-1}, characteristic of in-plane stretching of sp2 carbons of aromatics and olefins

forming well-structured coke or graphite-like structures and (v) D2 at 1610 cm^{-1}, attributed to disordered aromatic structures [33]. One example of deconvolution is shown in Figure 13.

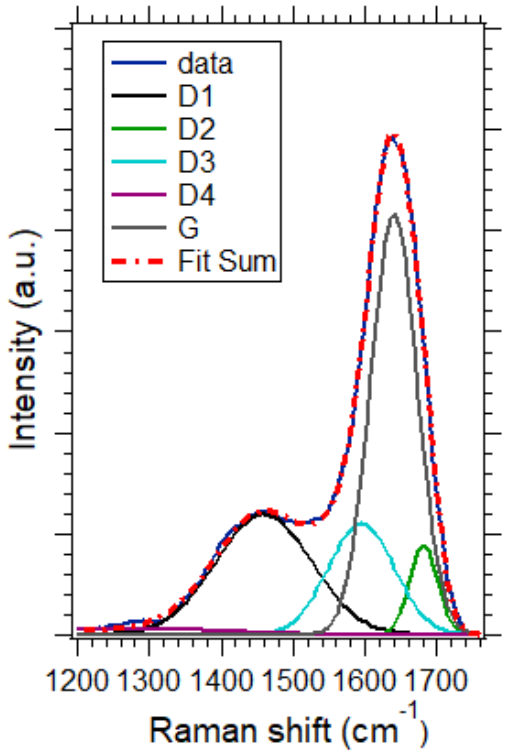

Figure 13 UV-Raman spectra for the SCD/SCW coke 2 h deconvoluted in Gaussian peaks

Figure 14 shows a plot of (D1+D4)/G versus reaction time for the coke produced in the presence of SCW. (D1+D4)/G varies inversely with cluster size. It was observed that (D1+D4)/G decreased, which suggests an increase in cluster size. However, it is important to mention that it is a modest increase in cluster size (from 1 aromatic ring to 2 or 3 aromatic rings).

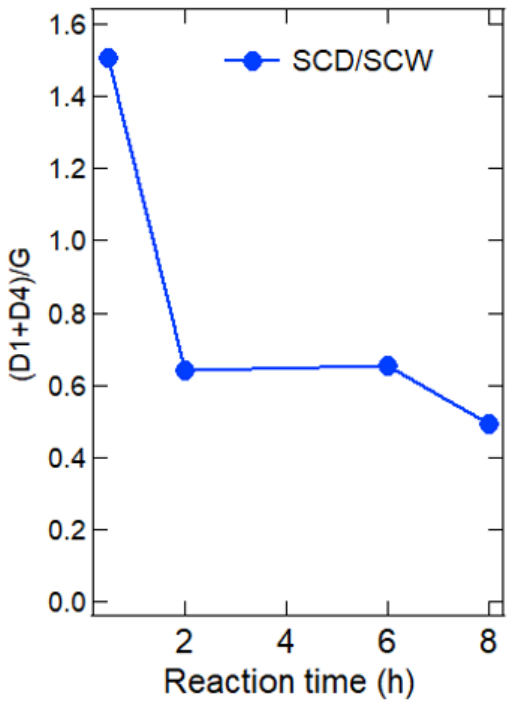

Figure 14 (D1+D4)/G versus reaction time

Conclusions

SCW reduced coke formation by an order of magnitude or more.

Coke produced in the absence of SCW was formed by PHAs with more than 4 aromatic rings containing alkyl side chains.

Coke produced in the presence of SCW was formed by 1 to 3 aromatic rings.

4.2 Specific Aim 2 - SCW can decrease Bronsted acidity of ZSM-5, which will decrease coke formation

To differentiate between the effect of SCW on ZSM-5 Bronsted acid sites (BASs) and the effect in coke formation another experiment was performed and was based in the pretreatment of the catalyst in SCW for 0 and 2 h for posterior use in the cracking of dodecane in the absence of water. Here, “0 hours” implies that the catalyst was placed in the reactor with water at room temperature, the temperature increased to 400 °C at a pressure greater than the critical pressure and then the reactor temperature was immediately cooled to room temperature; materials obtained from this test are termed ZSM-5 (SCW 0). The 2 h treatment was a more aggressive test, which is expected to decrease the BASs by approximately 90%; materials obtained from this test are termed ZSM-5 (SCW 2).

Figure 15 summarizes the coke quantification for the zeolites pretreated in SCW and then used in dodecane only. It was observed that the pretreated zeolites produced much less coke than the parent ZSM-5 treated in SCD, which was expected from consideration of the role of BASs in coke formation.

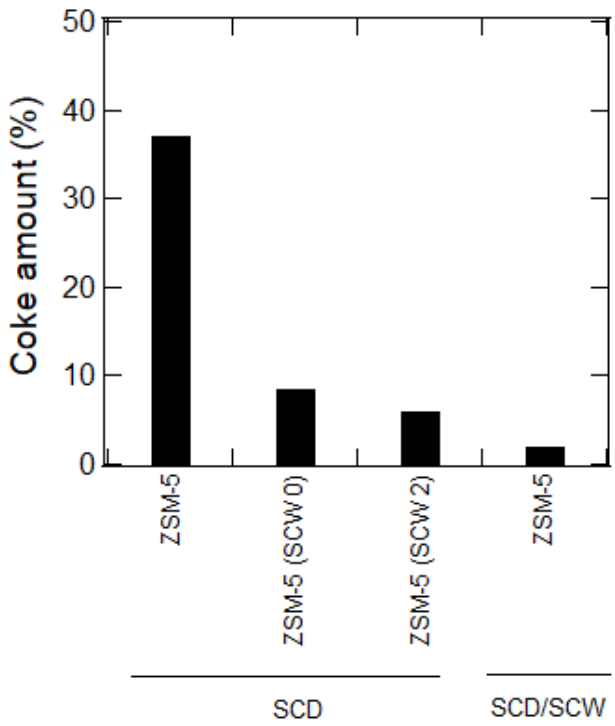

Figure 15 Coke amount for pretreated zeolites

Figure 16 shows the ATR-IR spectra obtained for the coke produced with the pretreated zeolites in comparison with the ZSM-5 treated in SCD/SCW and SCD. ATR-IR indicates that the composition of coked formed by SCW pretreated ZSM-5 is intermediate to that formed by the original ZSM-5 in the absence and presence of water. Coke formed with the pretreated zeolites contains both aromatic C-H and aromatic C-C content like coke formed on original ZSM-5 in the absence of water and CH_3 content as coke formed on original ZSM-5 in the presence of water. However, coke formed on SCW pretreated ZSM-5 did not show the same composition observed for the coke formed by original ZSM-5 in the presence of water, implying a chemical role of water on coke formation.

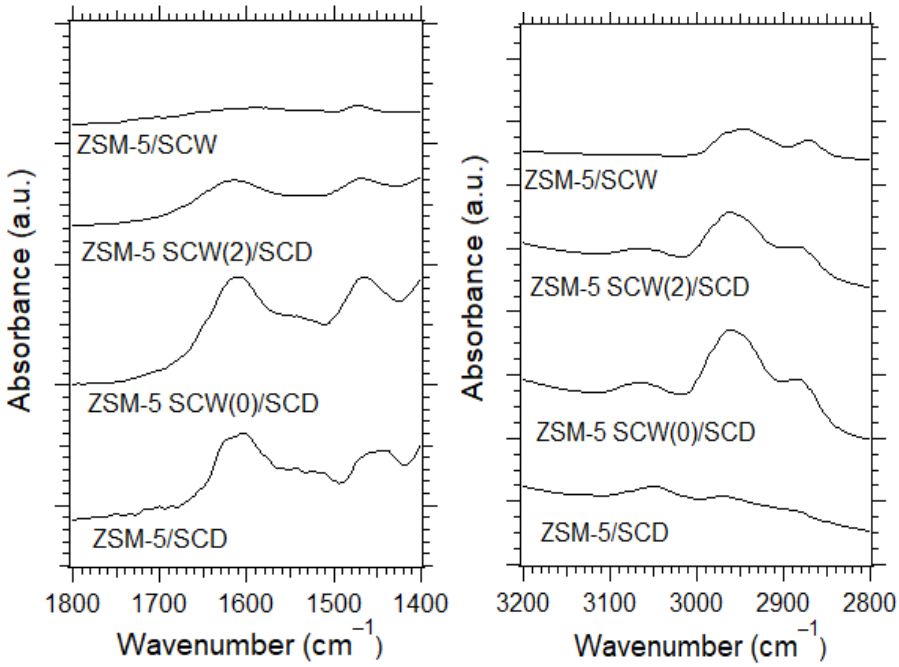

Figure 16 ATR-IR spectra for the coke produced with the pretreated zeolites

Figure 17 indicates the solid-state ^{13}C NMR with multi cross-polarization (Multi CP) data obtained for the coke produced with the pretreated catalysts. It was observed in the spectra saturated aliphatic carbon species due to reactant inside the pores and aromatic carbon attributed to coke constituents.

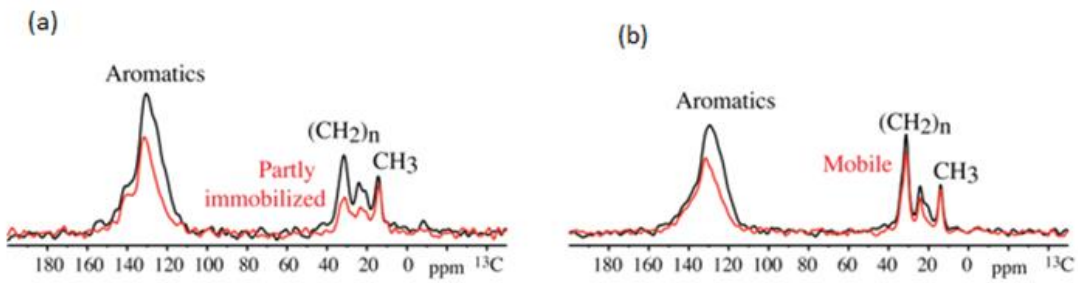

Figure 17 13C NMR spectra for (a) SCW(0)/SCD coke and (b) SCW(2)/SCD coke

Conclusions

Pre-treatment of the ZSM-5 catalysts in SCW reduced coke formation due to the removal of Bronsted acidity of the catalyst, which plays a key role in the mechanism of coke formation.

Coke produced with pre-treated zeolites had features of the coke produced in the presence and absence of SCW with the fresh zeolites.

4.3 Specific Aim 3- SCW can promote coke gasification in the presence of ZSM-5, which would decrease its quantity

In the literature, SCW has been used to decompose different carbon rich feedstocks into gaseous products (CH_4, H_2, CO_2 and CO). According to the process conditions, it is possible to differentiate three categories [34]:

1. High temperatures (500-700 °C) without catalysts or with homogeneous catalysts for H_2 production

2. Moderate temperatures (374-500 °C) with catalysts for CH_4 production

3. Low-moderate temperatures (< 374 °C, subcritical water) with catalysts for CH_4 production

In the present research, coke was gasified in SCW (400 ^{o}C) in the presence of ZSM-5 for 2 h to verify if coke formation could be restricted in SCW due to its gasification effects.

The amount of coke recorded before and after the gasification in SCW by TPO analysis is shown in Figure 18. It was observed that SCW promoted a partial coke gasification (10%).

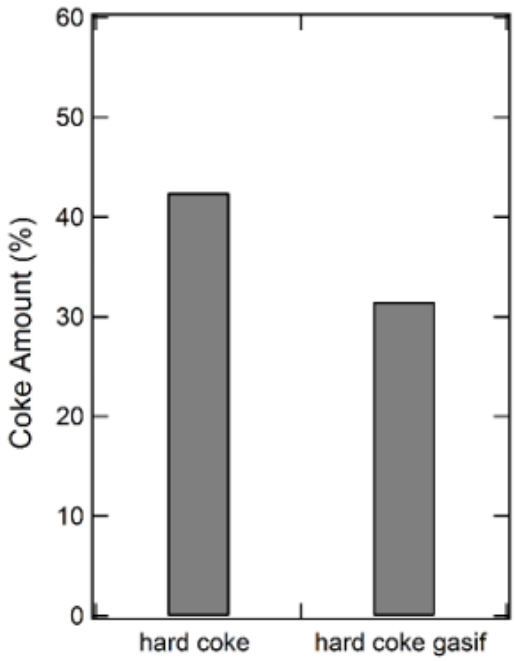

Figure 18 TPO analysis of the coke gasified in SCW at 400 ºC for 2h

The analysis of the gases for the gasification experiment is shown in Figure 19. It was verified that the main gas formed was CH_4, but CO_2, CO and other heavy gases were also identified.

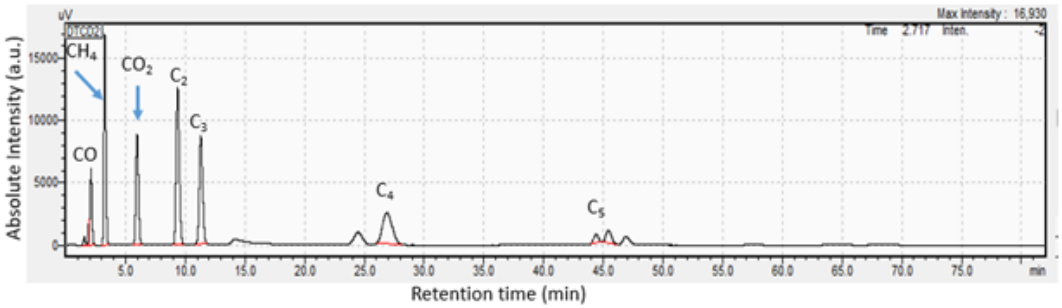

Figure 19 GC-TCD analysis for the gasification experiment

As mentioned before, high gasification temperatures favor water-gas shift reaction resulting in greater yields of H_2, while low temperatures favor methanation. The gas formation can be represented by the reactions below:

$$C + H_2O \longrightarrow CO + H_2$$

$$CO + H_2O \longrightarrow CO_2 + H_2 \quad \text{Water-Gas Shift}$$

$$CO + 3\,H_2 \longrightarrow CH_4 + H_2O \quad \text{Methanation}$$

Conclusions

SCW promoted partial gasification of coke in the presence of ZSM-5. The main gas formed was methane. This partial gasification effect of SCW can contribute to decrease coke formation.

4.4 Specific Aim 4: Coke deposits produced in the presence and absence of SCW can affect differently ZSM-5 activity

Coked zeolites produced in the presence and absence of SCW during a reaction time of 2 h were tested in ethanol dehydration reaction at 350 °C to measure how SCD/SCW coke formed could impact ZSM-5 activity.

Figure 20 shows the ethylene TOF ratio de-coked/coked calculated for the SCD/SCW and SCD catalysts. It was possible to observe that SCD/SCW deactivated less the catalyst because the coked SCD/SCW catalyst had almost the same activity of the de-coked SCD/SCW catalyst.

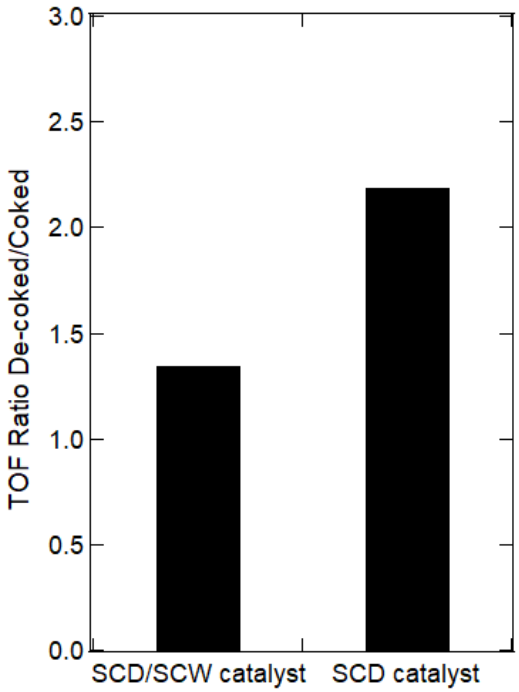

Figure 20 Ethylene TOF ratio de-coked/coked for SCW/SCD and SCD catalyst

SCD/SCW coke used in ethanol dehydration reaction was also analyzed by TPO to verify if the coke was being removed during the experiment and because of this the activity of the coked and de-coked catalysts was almost the same. According to the TPO

analysis shown in Figure 21, the amount of coke before the experiment was 2 % and after 1.6 %. Based on this, it was concluded that the SCD/SCW coke maintained stable during the ethanol dehydration reaction.

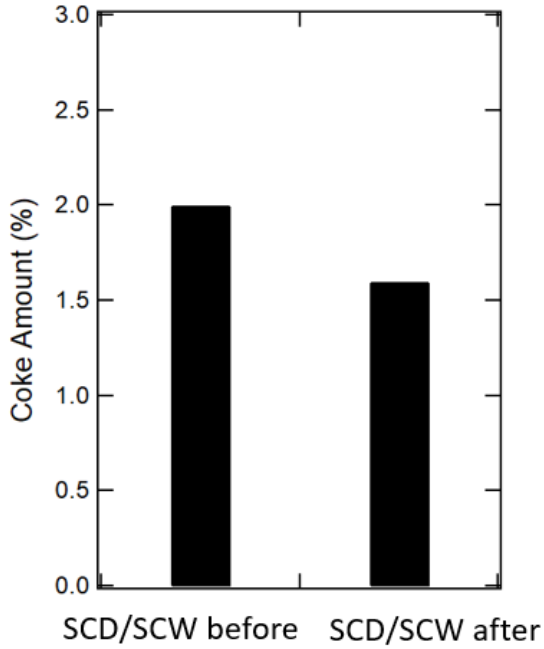

Figure 21 TPO SCD/SCW coke before and after ethanol dehydration reaction

Conclusions

SCD/SCW coke formed impacted less the activity of ZSM-5 during test in ethanol dehydration reaction than SCD coke.

CHAPTER 5

CONCLUSIONS

Based on the results presented, coke produced in the absence of SCW was formed by PHAs with more than 4 aromatic rings containing alkyl side chains, while coke produced in the presence of SCW was formed by 1 to 3 aromatic rings. It was also observed that SCW impacted coke formation by decreasing Bronsted acid sites of the catalyst and by promoting coke gasification in the presence of ZSM-5. Finally, it was observed that SCD/SCW coke deactivated less the catalyst than SCD coke.

REFERENCES

[1] Liu, H., Diao, Z., Liu, G., Wang, L., & Zhang, X. (2017). Catalytic cracking of n-dodecane over hierarchical HZSM-5 zeolites synthesized by double-template method. Journal of Porous Materials, 24(6), 1679–1687.

[2] Lv, J., Hua, Z., Ge, T., Zhou, J., Zhou, J., Liu, Z., … Shi, J. (2017). Phosphorus modified hierarchically structured ZSM-5 zeolites for enhanced hydrothermal stability and intensified propylene production from 1-butene cracking. Microporous and Mesoporous Materials, 247, 31–37.

[3] Alsobaai, A. M., Zakaria, R., & Hameed, B. H. (2007). Gas oil hydrocracking on NiW/USY catalyst: Effect of tungsten and nickel loading. Chemical Engineering Journal, 132(1–3), 77–83.

[4] Meng, J., Wang, Z., Ma, Y., & Lu, J. (2017). Hydrocracking of low-temperature coal tar over NiMo/Beta-KIT-6 catalyst to produce gasoline oil. Fuel Processing Technology, 165, 62–71.

[5] Zheng, J., Dong, J. L., Xu, Q. H., Liu, Y., & Yan, A. Z. (1995). Comparison between β and L zeolites supported platinum for n-hexane aromatization. Applied Catalysis A, General, 126(1), 141–152.

[6] Chen, X., Dong, M., Niu, X., Wang, K., Chen, G., Fan, W., … Qin, Z. (2015). Influence of Zn species in HZSM-5 on ethylene aromatization. Cuihua Xuebao/Chinese Journal of Catalysis, 36(6), 880–888.

[7] Bauer, F., Chen, W. H., Ernst, H., Huang, S. J., Freyer, A., & Liu, S. Bin. (2004). Selectivity improvement in xylene isomerization. Microporous and Mesoporous Materials, 72(1–3), 81–89.

[8] Barsi, F. V., & Cardoso, D. (2009). Bimetallic Pt-Ni catalysts supported on usy zeolite for n-hexane isomerization. Brazilian Journal of Chemical Engineering, 26(2), 353–360.

[9] Yoo, K., Burckle, E. C., & Smirniotis, P. G. (2002). Isobutane/2-butene alkylation using large pore zeolites: Influence of pore structure on activity and selectivity. Journal of Catalysis, 211(1), 6–18.

[10] Nivarthy, G. S., Feller, A., Seshan, K., & Lercher, J. A. (2000). Alkylation of isobutane with light olefins catalyzed by zeolite beta. Microporous and Mesoporous Materials, 35–36, 75–87.

[11] Shao, J., Fu, T., Chang, J., Wan, W., Qi, R., & Li, Z. (2017). Effect of ZSM-5 crystal size on its catalytic properties for conversion of methanol to gasoline. Journal of Fuel Chemistry and Technology, 45(1), 75–83.

[12] Soltanali, S., Halladj, R., Rashidi, A., & Hajjar, Z. (2017). The effect of HZSM-5 catalyst particle size on gasoline selectivity in methanol to gasoline conversion process. Powder Technology, 320, 696–702.

[13] Li, X., Su, L., Wang, Y., Yu, Y., Wang, C., Li, X., & Wang, Z. (2012). Catalytic fast pyrolysis of Kraft lignin with HZSM-5 zeolite for producing aromatic hydrocarbons. Frontiers of Environmental Science and Engineering in China, 6(3), 295–303.

[14] Zhang, H., Zheng, J., & Xiao, R. (2013). Catalytic pyrolysis of willow wood with Me/ZSM-5 (Me = Mg, K, Fe, Ga, Ni) to produce aromatics and olefins. Bio Resources, 8(4), 5612–5621.

[15] Anand, V., Sunjeev, V., & Vinu, R. (2016). Catalytic fast pyrolysis of Arthrospira platensis (spirulina) algae using zeolites. Journal of Analytical and Applied Pyrolysis, 118, 298–307.

[16] Kim, B. S., Kim, Y. M., Jae, J., Watanabe, C., Kim, S., Jung, S. C., … Park, Y. K. (2015). Pyrolysis and catalytic upgrading of Citrus unshiu peel. Bioresource Technology, 194, 312–319.

[17] Wang, B., & Manos, G. (2008). Deactivation studies during 1-pentene reactions over HUSY zeolite. Chemical Engineering Journal, 142(2), 217–223.

[18] Paweewan, B., Barrie, P. J., & Gladden, L. F. (1999). Coking and deactivation during n-hexane cracking in ultrastable zeolite Y. Applied Catalysis A: General, 185(2), 259–268.

[19] Lee, K. Y., Kang, M. Y., & Ihm, S. K. (2012). Deactivation by coke deposition on the HZSM-5 catalysts in the methanol-to-hydrocarbon conversion. Journal of Physics and Chemistry of Solids, 73(12), 1542–1545.

[20] Querini, C. A., & Roa, E. (1997). Deactivation of solid acid catalysts during isobutane alkylation with C4 olefins. Applied Catalysis A: General, 163(1–2), 199–215.

[21] Han, L., Zhang, R., & Bi, J. (2008). Upgrading of coal-tar pitch in supercritical water. Journal of Fuel Chemistry and Technology, 36(1), 1–5.

[22] Morimoto, M., Sugimoto, Y., Saotome, Y., Sato, S., & Takanohashi, T. (2010). Effect of supercritical water on upgrading reaction of oil sand bitumen. Journal of Supercritical Fluids, 55(1), 223–231.

[23] Cheng, Z. M.; Ding, Y.; Zhao, L. Q.; Yuan, P. Q.; Yuan, W. K. (2009). Effects of supercritical water in vacuum residue upgrading. Energy Fuels, 23, 3178−3183.

[24] Yuan, P. Q., Zhu, C. C., Liu, Y., Bai, F., Cheng, Z. M., & Yuan, W. K. (2011). Solvation of hydrocarbon radicals in sub-CW and SCW: An ab initio MD study. Journal of Supercritical Fluids, 58(1), 93–98.

[25] Zhao, Y., Wei, F., & Yu, Y. (2008). Inhibition of Coke Formation in Cracking of 2-Methylpentane on USHY by Addition of Steam. Chinese Journal of Chemical Engineering, 16(5), 726–732.

[26] Daramola, M. O., Aransiola, E. F., & Ojumu, T. V. (2012). Potential applications of zeolite membranes in reaction coupling separation processes. Materials, 5(11), 2101–2136.

[27] Guisnet, M., & Magnoux, P. (2001). Organic Chemistry of Coke Formation. Appl. Catal., 212, 83.

[28] Li, J., Xiong, G., Feng, Z., Liu, Z., Xin, Q., & Li, C. (2000). Coke formation during the methanol conversion to olefins in zeolites studied by UV Raman spectroscopy. Microporous and Mesoporous Materials, 39(1–2), 275–280.

[29] Du, S., Gamliel, D. P., Giotto, M. V., Valla, J. A., & Bollas, G. M. (2016). Coke formation of model compounds relevant to pyrolysis bio-oil over ZSM-5. Applied Catalysis A: General, 513, 67–81.

[30] Cerqueira, H. S., Magnoux, P., Martin, D., & Guisnet, M. (2001). Coke formation and coke profiles during the transformation of various reactants at 450 °C over a USHY zeolite. Applied Catalysis A: General, 208(1–2), 359–367.

[31] Johnson, R. L., & Schmidt-Rohr, K. (2014). Quantitative solid-state 13C NMR with signal enhancement by multiple cross polarization. Journal of Magnetic Resonance, 239, 44–49.

[32] Castaño, P., Elordi, G., Olazar, M., Aguayo, A. T., Pawelec, B., & Bilbao, J. (2011). Insights into the coke deposited on HZSM-5, Hβ and HY zeolites during the cracking of polyethylene. Applied Catalysis B: Environmental, 104(1–2), 91–100.

[33] Timko, M. T., Maag, A. R., Venegas, J. M., McKeogh, B., Yang, Z., Tompsett, G. A., … Greenaway, F. T. (2016). Spectroscopic tracking of

mechanochemical reactivity and modification of a hydrothermal char. RSC Advances, 6(15), 12021–12031.

[34] Jin, H., Liu, S., Wei, W., Zhang, D., Cheng, Z., & Guo, L. (2015). Experimental Investigation on Hydrogen Production by Anthracene Gasification in Supercritical Water. Energy & Fuels, 29(10), 6342–6346.

APPENDIX A

ATR-IR Peak Fitting

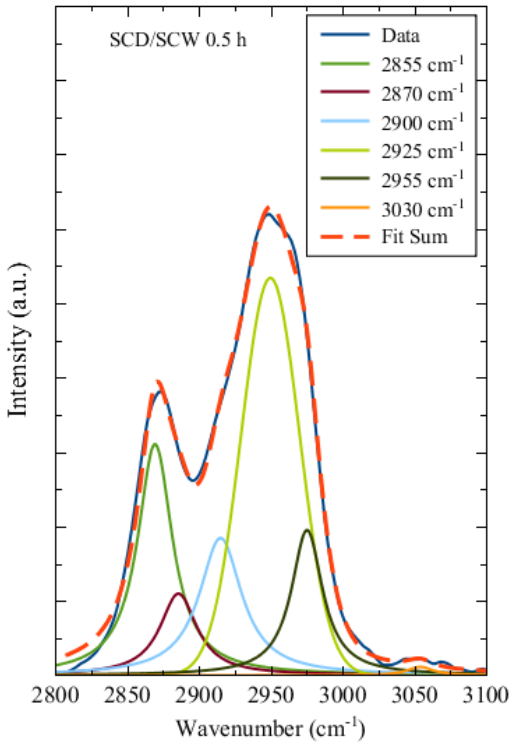

Figure A1 ATR-IR spectra for the SCD/SCW coke 0.5 h deconvoluted in Lorentzian peaks

Table A1 ATR-IR peak fitting description for SCD/SCW coke 0.5 h

Curve Number	Position (cm^{-1})	Area	% Area
1	2855	0.0287	19.6946
2	2870	0.0220	15.0840
3	2900	0.0238	16.2949
4	2925	0.0545	37.3357
5	2955	0.0161	11.0623
6	3030	0.0008	0.5286
Total		**0.1459**	
Coefficient of Determination R^2	**9.99E-01**		

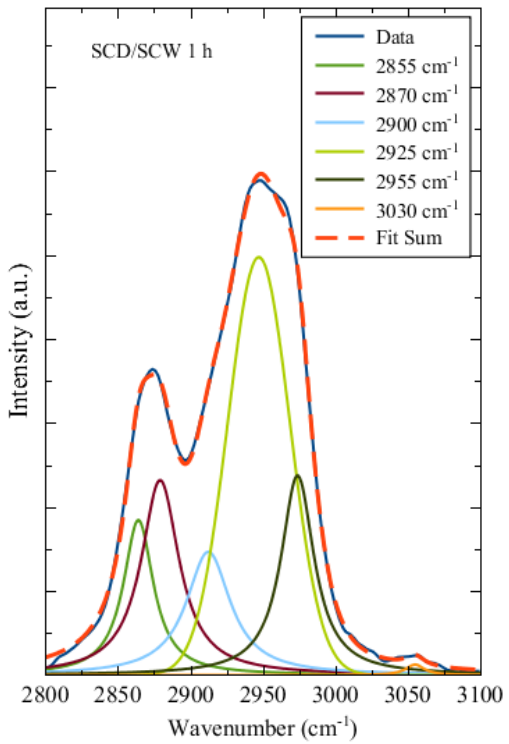

Figure A2 ATR-IR spectra for the SCD/SCW coke 1 h deconvoluted in Lorentzian peaks

Table A2 ATR-IR peak fitting description for SCD/SCW coke 1 h

Curve Number	Position (cm^{-1})	Area	% Area
1	2855	0.0145	11.2524
2	2870	0.0232	17.9373
3	2900	0.0170	13.1675
4	2925	0.0533	41.2310
5	2955	0.0206	15.9446
6	3030	0.0006	0.4672
Total		**0.1293**	
Coefficient of Determination R^2	**9.99E-01**		

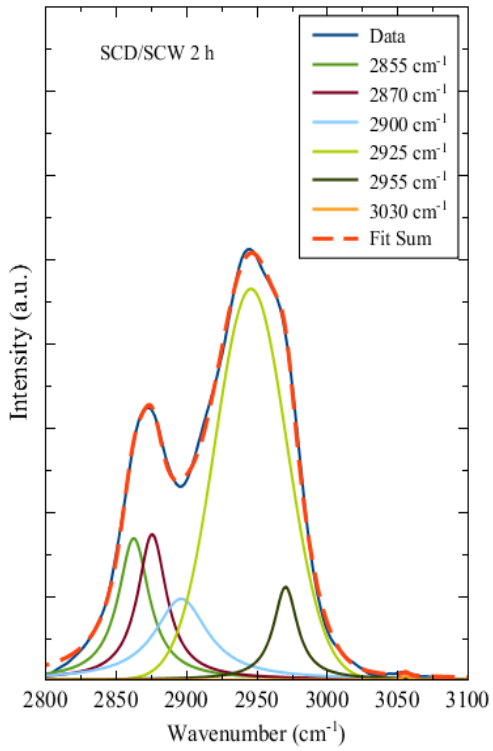

Figure A3 ATR-IR spectra for the SCD/SCW coke 2 h deconvoluted in Lorentzian peaks

Table A3 ATR-IR Peak fitting description for SCD/SCW coke 2 h

Curve Number	Position (cm^{-1})	Area	% Area
1	2855	0.0353	13.0926
2	2870	0.0339	12.5792
3	2900	0.0344	12.7592
4	2925	0.1483	54.9808
5	2955	0.0178	6.5882
6	3030	0.0000	0.0000
Total		**0.2698**	
Coefficient of Determination R^2	**9.99E-01**		

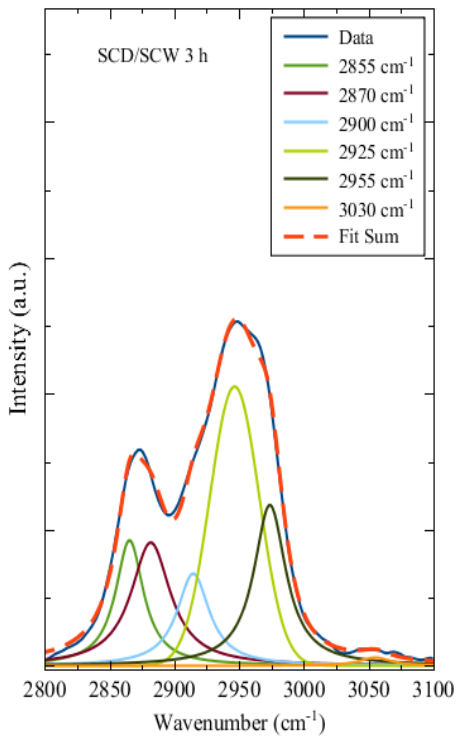

Figure A4 ATR-IR spectra for the SCD/SCW coke 3 h deconvoluted in Lorentzian peaks

Table A4 ATR-IR peak fitting description for SCD/SCW coke 3 h

Curve Number	Position (cm^{-1})	Area	% Area
1	2855	0.0190	13.5906
2	2870	0.0263	18.8400
3	2900	0.0161	11.5419
4	2925	0.0491	35.1016
5	2955	0.0279	19.9341
6	3030	0.0014	0.9916
Total		**0.1398**	
Coefficient of Determination R^2	**9.99E-01**		

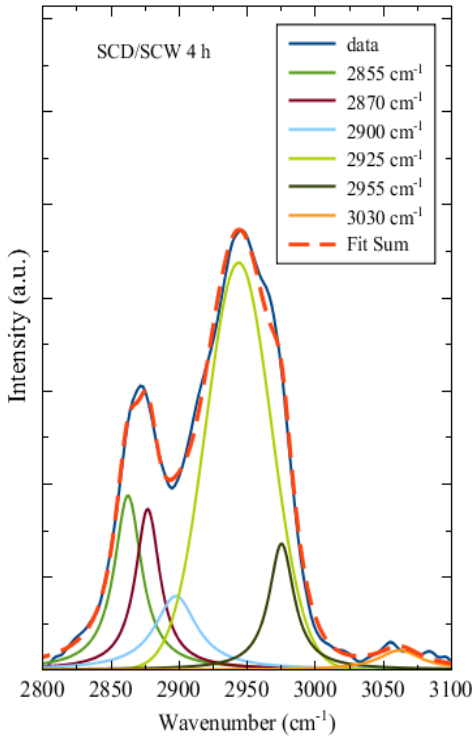

Figure A5 ATR-IR spectra for the SCD/SCW coke 4 h deconvoluted in Lorentzian peaks

Table A5 ATR-IR peak fitting description for SCD/SCW coke 4 h

Curve Number	Position (cm^{-1})	Area	% Area
1	2855	0.0143	14.3358
2	2870	0.0119	11.9298
3	2900	0.0093	9.3133
4	2925	0.0523	52.4311
5	2955	0.0095	9.4837
6	3030	0.0025	2.5063
Total		**0.0998**	
Coefficient of Determination R^2	**9.97E-01**		

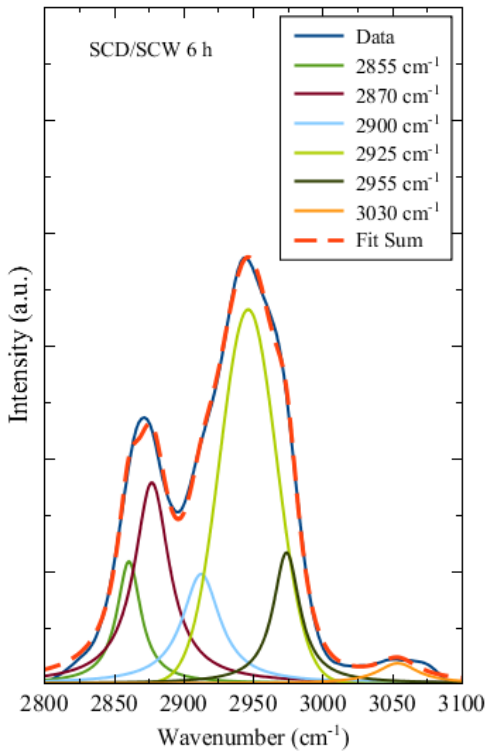

Figure A6 ATR-IR spectra for the SCD/SCW coke 6 h deconvoluted in Lorentzian peaks

Table A6 ATR-IR peak fitting description for SCD/SCW coke 6 h

Curve Number	Position (cm^{-1})	Area	% Area
1	2855	0.0178	9.0818
2	2870	0.0427	21.7752
3	2900	0.0251	12.8114
4	2925	0.0844	43.0087
5	2955	0.0211	10.7630
6	3030	0.0050	2.5599
Total		**0.1962**	
Coefficient of Determination R^2	**9.98E-01**		

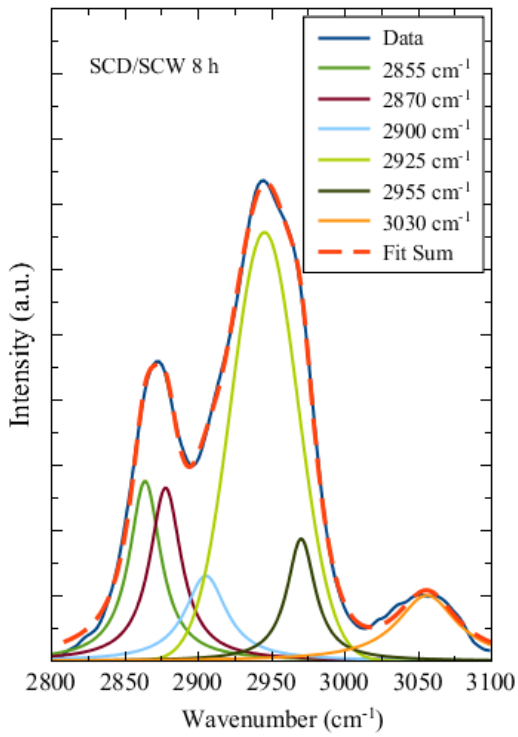

Figure A7 ATR-IR spectra for the SCD/SCW coke 8 h deconvoluted in Lorentzian peaks

Table A7 ATR-IR peak fitting description for SCD/SCW coke 8 h

Curve Number	Position (cm^{-1})	Area	% Area
1	2855	0.0225	13.8214
2	2870	0.0218	13.3909
3	2900	0.0140	8.6346
4	2925	0.0748	46.0220
5	2955	0.0137	8.4421
6	3030	0.0158	9.6889
Total		**0.1626**	
Coefficient of Determination R^2	**9.98E-01**		

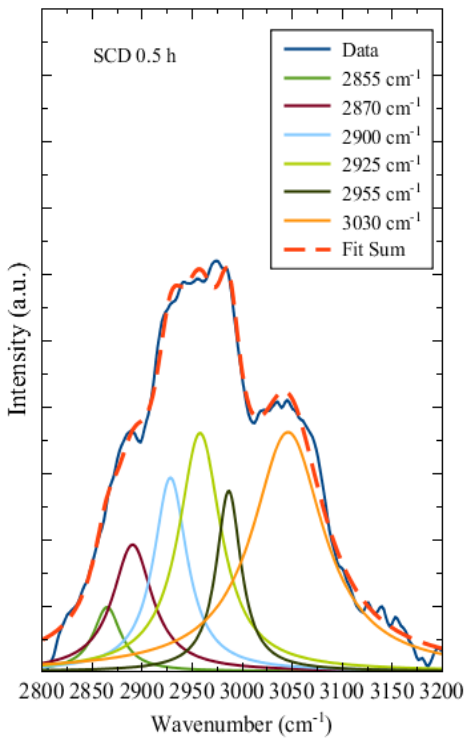

Figure A8 ATR-IR spectra for the SCD coke 0.5 h deconvoluted in Lorentzian peaks

Table A8 ATR-IR peak fitting description for SCD coke 0.5 h

Curve Number	Position (cm^{-1})	Area	% Area
1	2855	0.0025	3.9377
2	2870	0.0072	11.1580
3	2900	0.0093	14.4107
4	2925	0.0146	22.5757
5	2955	0.0065	10.0179
6	3030	0.0245	37.9000
Total		**0.0645**	
Coefficient of Determination R^2	**9.91E-01**		

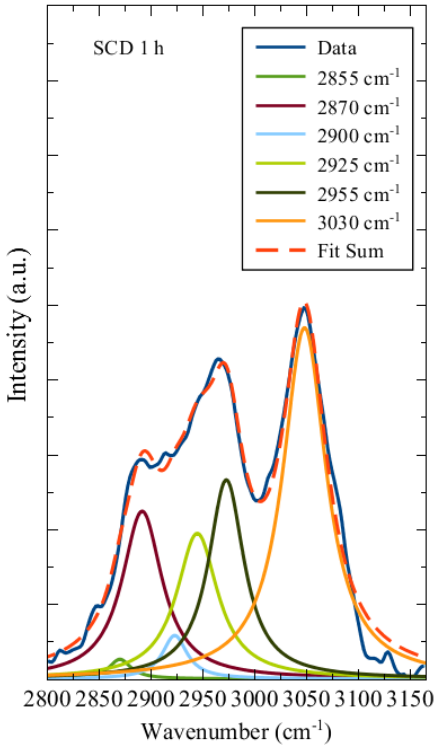

Figure A9 ATR-IR spectra for the SCD coke 1 h deconvoluted in Lorentzian peaks

Table A9 ATR-IR peak fitting description for SCD coke 1 h

Curve Number	Position (cm^{-1})	Area	% Area
1	2855	0.0010	1.1259
2	2870	0.0166	18.4084
3	2900	0.0025	2.7805
4	2925	0.0151	16.8180
5	2955	0.0172	19.1001
6	3030	0.0376	41.7671
Total		**0.0900**	
Coefficient of Determination R^2	**9.93E-01**		

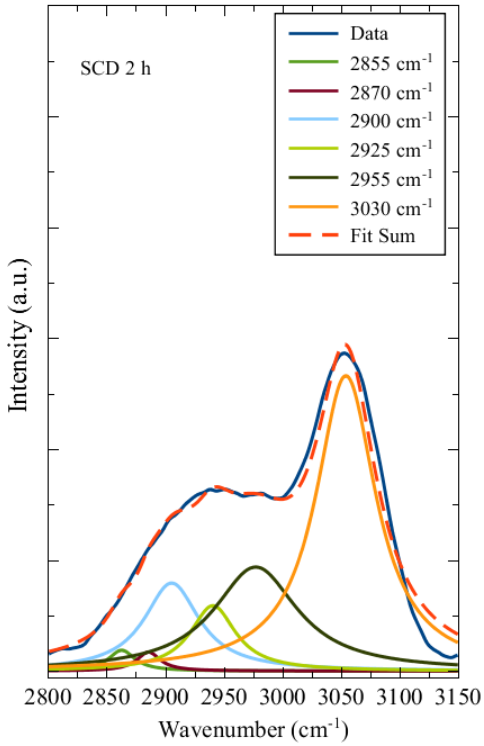

Figure A10 ATR-IR spectra for the SCD coke 2 h deconvoluted in Lorentzian peaks

Table A10 ATR-IR peak fitting description for SCD coke 2 h

Curve Number	Position (cm^{-1})	Area	% Area
1	2855	0.0016	1.5518
2	2870	0.0013	1.2578
3	2900	0.0142	13.7029
4	2925	0.0087	8.3751
5	2955	0.0256	24.6647
6	3030	0.0523	50.4476
Total		**0.1037**	
Coefficient of Determination R^2	**9.97E-01**		

APPENDIX B

DR-UV-vis Peak Fitting

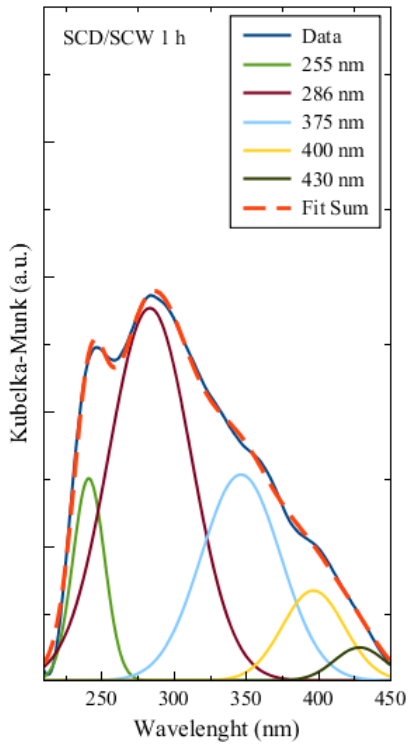

Figure B1 DR-UV-vis spectra for the SCD/SCW coke 1 h deconvoluted in Gaussian peaks

Table B1 DR-UV-vis peak fitting description for SCD/SCW coke 1 h

Curve Number	Position (nm)	Area	% Area
1	255	0.2056	10.5185
2	286	0.9894	50.6101
4	375	0.5269	26.9536
5	400	0.1794	9.1767
6	430	0.0536	2.7410
Total		1.9550	
Coefficient of Determination R^2	**9.94E-01**		

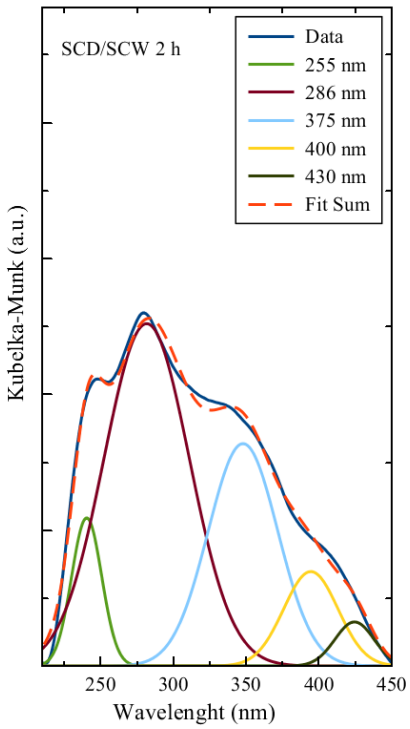

Figure B2 DR-UV-vis spectra for the SCD/SCW coke 2 h deconvoluted in Gaussian peaks

Table B2 DR-UV-vis peak fitting description for SCD/SCW coke 2 h

Curve Number	Position (nm)	Area	% Area
1	255	0.1413	7.9548
2	286	0.9264	52.1479
4	375	0.4916	27.6760
5	400	0.1624	9.1396
6	430	0.0547	3.0816
Total		1.7764	
Coefficient of Determination R^2	**9.94E-01**		

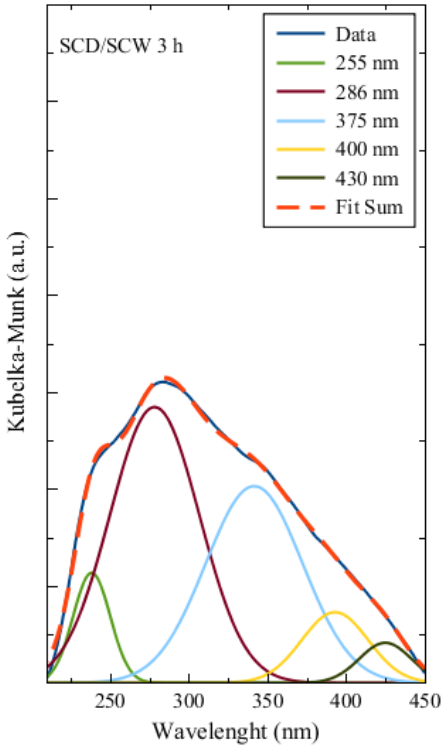

Figure B3 DR-UV-vis spectra for the SCD/SCW coke 3 h deconvoluted in Gaussian peaks

Table B3 DR-UV-vis peak fitting description for SCD/SCW coke 3 h

Curve Number	Position (nm)	Area	% Area
1	255	0.1677	7.4641
2	286	1.0164	45.2523
4	375	0.7840	34.9033
5	400	0.1929	8.5873
6	430	0.0852	3.7931
Total		2.2461	
Coefficient of Determination R^2	**9.98E-01**		

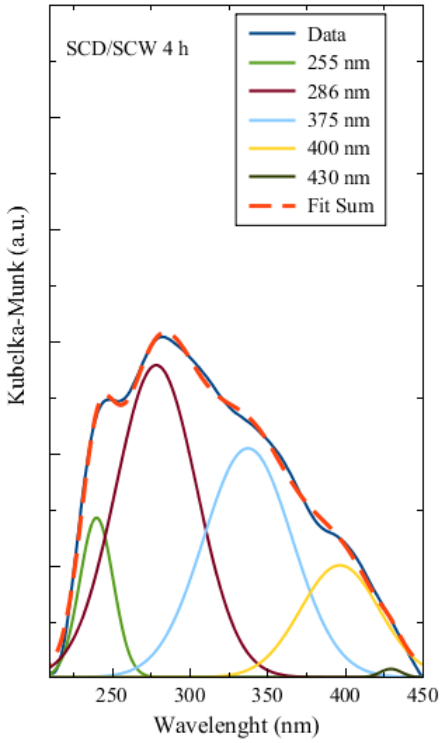

Figure B4 DR-UV-vis spectra for the SCD/SCW coke 4 h deconvoluted in Gaussian peaks

Table B4 DR-UV-vis peak fitting description for SCD/SCW coke 4 h

Curve Number	Position (nm)	Area	% Area
1	255	0.1921	8.9084
2	286	0.9096	42.1873
4	375	0.7300	33.8586
5	400	0.3180	14.7466
6	430	0.0065	0.2992
Total		2.1561	
Coefficient of Determination R^2	**9.97E-01**		

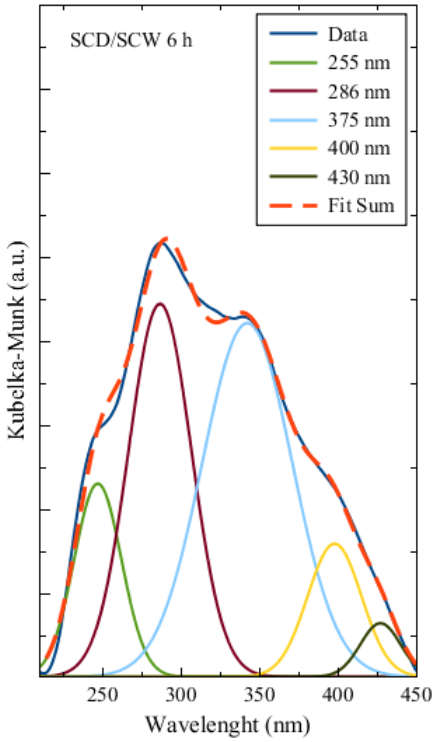

Figure B5 DR-UV-vis spectra for the SCD/SCW coke 6 h deconvoluted in Gaussian peaks

Table B5 DR-UV-vis peak fitting description for SCD/SCW coke 6 h

Curve Number	Position (nm)	Area	% Area
1	255	0.1730	12.3556
2	286	0.4468	31.9111
4	375	0.6034	43.0962
5	400	0.1360	9.7145
6	430	0.0409	2.9225
Total		1.4002	
Coefficient of Determination R^2	**9.95E-01**		

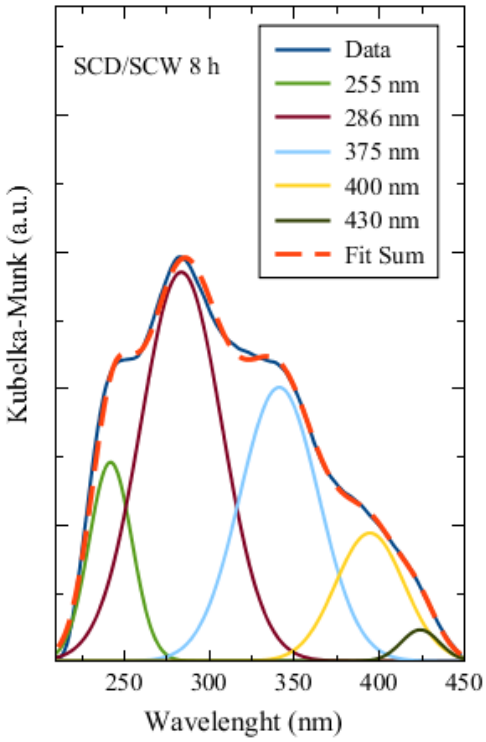

Figure B6 DR-UV-vis spectra for the SCD/SCW coke 8 h deconvoluted in Gaussian peaks

Table B6 DR-UV-vis peak fitting description for SCD/SCW coke 8 h

Curve Number	Position (nm)	Area	% Area
1	255	0.2369	12.2439
2	286	0.8497	43.9056
4	375	0.5805	29.9964
5	400	0.2362	12.2041
6	430	0.0319	1.6500
Total		1.9352	
Coefficient of Determination R^2	**9.97E-01**		

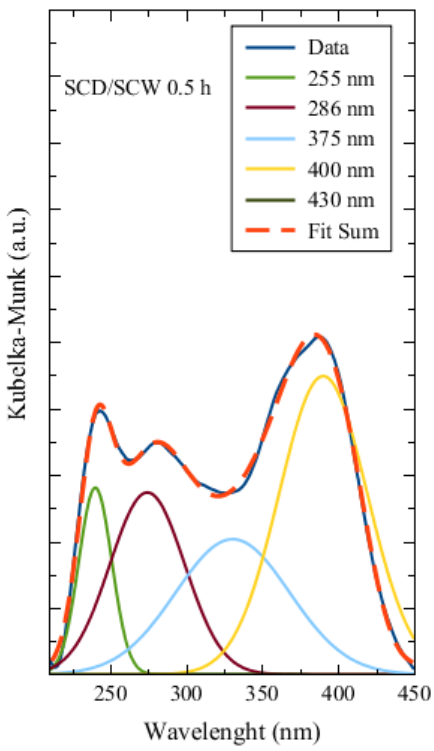

Figure B7 DR-UV-vis spectra for the SCD coke 0.5 h deconvoluted in Gaussian peaks

Table B7 DR-UV-vis peak fitting description for SCD coke 0.5 h

Curve Number	Position	Area	% Area
1	255	0.3826	10.0412
2	286	0.8417	22.0939
4	375	0.9551	25.0702
5	400	1.6304	42.7947
6	430	0.0000	0.0000
Total		3.8098	
Coefficient of Determination R^2	**9.96E-01**		

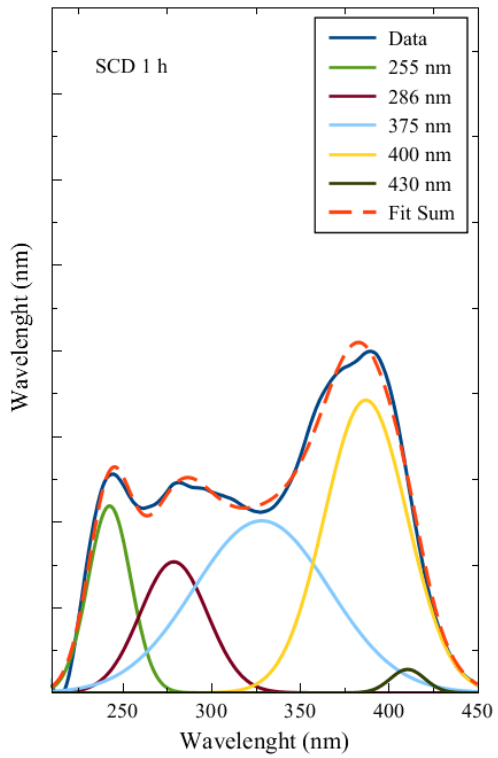

Figure B8 DR-UV-vis spectra for the SCD coke 1 h deconvoluted in Gaussian peaks

Table B8 DR-UV-vis peak fitting description for SCD coke 1 h

Curve Number	Position	Area	% Area
1	255	0.3298	12.2875
2	286	0.3631	13.5249
4	375	0.9612	35.8059
5	400	0.9971	37.1436
6	430	0.0332	1.2382
Total		2.6844	
Coefficient of Determination R^2	**9.91E-01**		

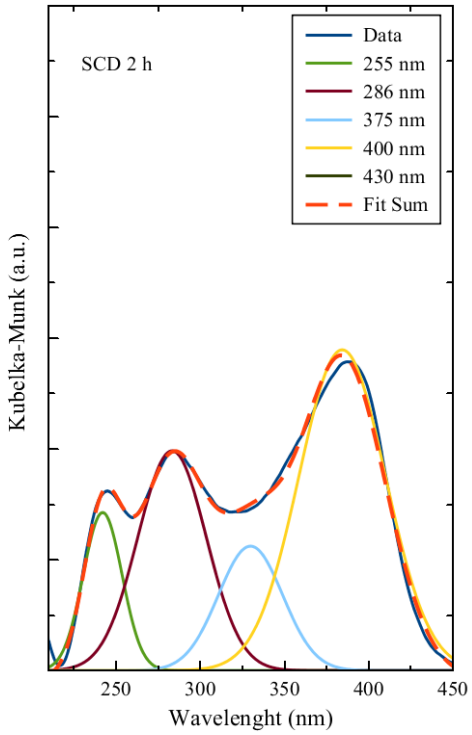

Figure B9 DR-UV-vis spectra for the SCD coke 2 h deconvoluted in Gaussian peaks

Table B9 DR-UV-vis peak fitting description for SCD coke 2 h

Curve Number	Position	Area	% Area
1	255	0.2059	10.7740
2	286	0.5059	26.4659
4	375	0.2685	14.0453
5	400	0.9312	48.7149
6	430	0.0000	0.0000
Total		1.9115	
Coefficient of Determination R^2	**9.91E-01**		

APPENDIX C

UV-Raman Peak Fitting

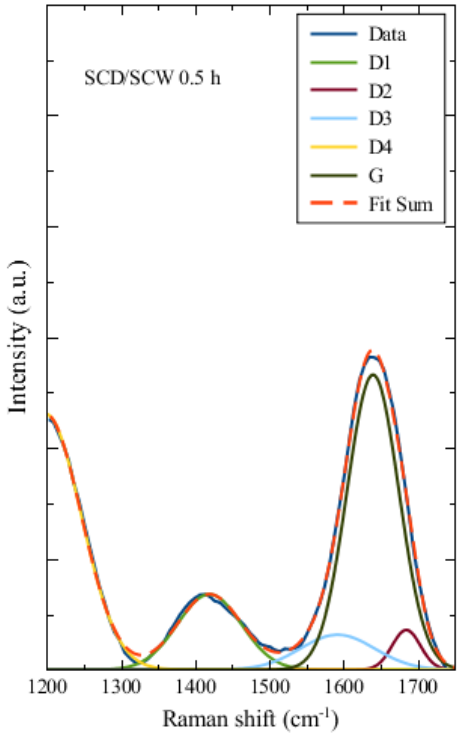

Figure C1 UV-Raman spectra for the SCD/SCW coke 0.5 h deconvoluted in Gaussian peaks

Table C1 UV-Raman peak fitting description for SCD/SCW coke 0.5 h

Curve Number	Position (cm^{-1})	Area	% Area
1	1350	3663.4576	11.4258
2	1600	857.3453	2.6739
3	1529	1977.5600	6.1677
4	1210	13908.1439	43.3776
5	1575	11656.4325	36.3548
Total		**32062.9392**	
Coefficient of Determination R^2	**9.98E-01**		

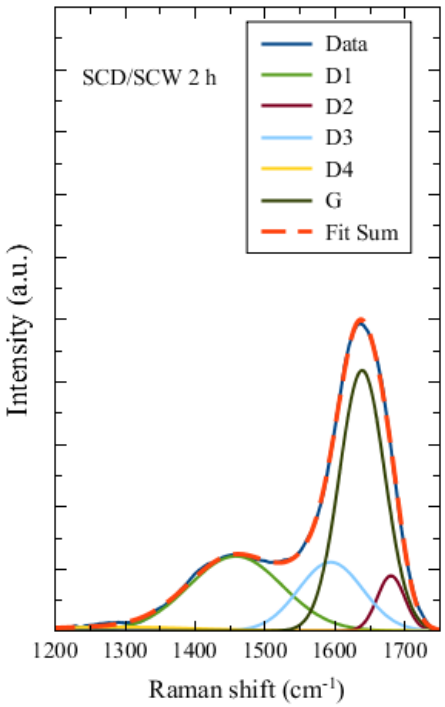

Figure C2 UV-Raman spectra for the SCD/SCW coke 2 h deconvoluted in Gaussian peaks

Table C2 UV-Raman peak fitting description for SCD/SCW coke 2 h

Curve Number	Position (cm^{-1})	Area	% Area
1	1350	10003.4720	27.4966
2	1600	2170.8901	5.9671
3	1529	6342.3379	17.4332
4	1210	896.4453	2.4641
5	1575	16967.5966	46.6390
Total		36380.7419	
Coefficient of Determination R^2	9.99E-01		

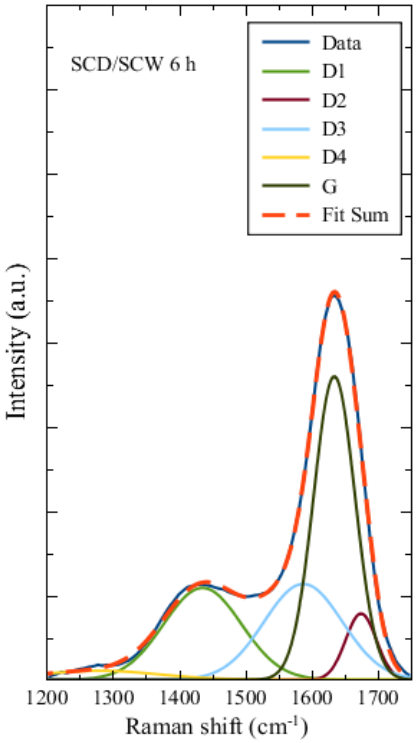

Figure C3 UV-Raman spectra for the SCD/SCW coke 6 h deconvoluted in Gaussian peaks

Table C3 UV-Raman peak fitting description for SCD/SCW coke 6 h

Curve Number	Position (cm^{-1})	Area	% Area
1	1350	15999.4590	23.5597
2	1600	4531.7239	6.6731
3	1529	16790.9322	24.7251
4	1210	2384.3001	3.5110
5	1575	28203.9545	41.5311
Total		**67910.3698**	
Coefficient of Determination R^2	**9.99E-01**		

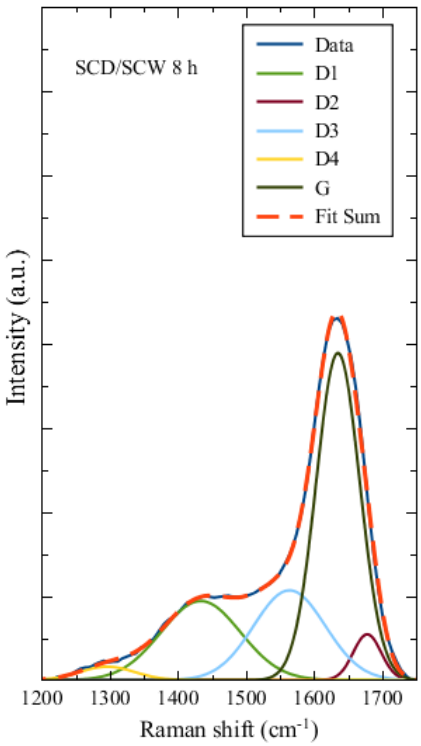

Figure C4 UV-Raman spectra for the SCD/SCW coke 8 h deconvoluted in Gaussian peaks

Table C4 UV-Raman peak fitting description for SCD/SCW coke 8 h

Curve Number	Position (cm^{-1})	Area	% Area
1	1350	13737.6065	21.6762
2	1600	2788.8697	4.4005
3	1529	14035.5811	22.1463
4	1210	1598.8475	2.5228
5	1575	31215.6677	49.2543
Total		**63376.5724**	
Coefficient of Determination R^2	**9.99E-01**		

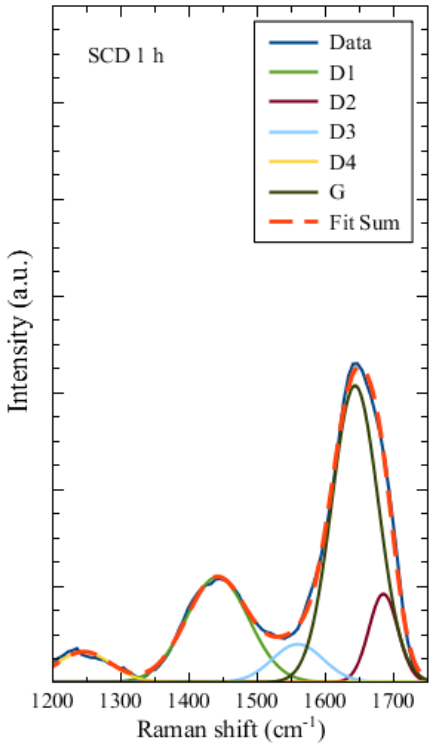

Figure C5 UV-Raman spectra for the SCD coke 1 h deconvoluted in Gaussian peaks

Table C5 UV-Raman peak fitting description for SCD coke 1 h

Curve Number	Position (cm^{-1})	Area	% Area
1	1350	6247.74	24.79
2	1600	2414.77	9.58
3	1529	1831.91	7.27
4	1210	1574.97	6.25
5	1575	13136.01	52.12
Total		**25205.40**	
Coefficient of Determination R^2	**9.97E-01**		